Supporting information for:

Are Actinyl Cations good Probes for Structure Determination in Solution by NMR?

Md. Ashraful Islam,[†] Matthieu Autillo,[‡] Clovis Poulin-Ponnelle,[‡] Christelle Tamain,[‡] Hélène Bolvin,[*,†] and Claude Berthon[*,‡]

†*Laboratoire de Chimie et Physique Quantiques, CNRS, Université Toulouse III, 118 route de Narbonne, 31062 Toulouse, France*

‡*CEA, DES, ISEC, DMRC, Univ. Montpellier, Bagnols sur Cèze 30207, France*

E-mail: bolvin@irsamc.ups-tlse.fr; claude.berthon@cea.fr

Contents

S1 Geometric structure of the complexes

Table S1: Crystallographic information for $An^{VI}O_2(TEDGA)_2(CF_3SO_3)_2$ compounds: A, B and C stand for An=U (CCDC: 2221521), Np (CCDC: 2221522) and Pu (CCDC: 2221523) respectively.

	A	B	C
	$C_{26}H_{48}F_6N_4O_{14}S_2U$	$C_{26}H_{48}F_6N_4O_{14}S_2Np$	$C_{26}H_{48}F_6N_4O_{14}S_2Pu$
Crystal colour	Yellow	Orange	Orange
Crystal size (μm)	200x180x140	75x25x10	440x140x120
Crystal system	Triclinic	Triclinic	Triclinic
Space group	$P\bar{1}$	$P\bar{1}$	$P\bar{1}$
Z	1	1	1
FW	1056.83	1055.8	1060.83
a	9.2787(5)	9.2890(3)	9.2992(4)
b	9.4523(5)	9.4848(4)	9.4826(5)
c	12.1763(6)	12.1496(5)	12.1431(6)
α	112.530(2)	112.722(2)	112.638(2)
β	103.302(2)	103.081(1)	102.943(1)
γ	93.887(2)	93.814(1)	93.797(1)
V (Å^3)	945.40(9)	947.51(7)	949.25(8)
Density (Mg.m−3)	1.856	1.85	1.856
Wavelength (Å)	0.71073	0.71073	0.71073
μ (mm^{-1})	4.499	2.948	1.942
Temperature (K)	100	100	100
2θ range (°)	1.885 – 30.541	2.363 – 28.360	2.361 – 30.565
L.S. parameters, p	296	323	323
R/Rw $[I > 2\sigma(I)]$	0.0303/0.1009	0.0137/0.0358	0.0140/0.0574
R/Rw (all data) $[I > 2\sigma(I)]$	0.0335/0.1160	0.0137/0.0358	0.0160/0.0706
Goof	1.248	1.117	1.325

Table S2: Crystallographic information for $U^{VI}O_2(TEDGA)_2(NO_3)_2$ (CCDC: 2221524) and $[U^{VI}O_2(TEDGA)(NO_3)_2](HCCl_3)$ (CCDC: 2221525) compounds noted E and F respectively.

	E	F
	$C_{24}H_{48}N_6O_{14}U$	$C_{13}H_{25}N_4O_{11}Cl_3U$
Crystal colour	Yellow	Yellow
Crystal size (mm)	230x50x50	170x160x130
Crystal system	Triclinic	Monoclinic
Space group	$P\overline{1}$	$P2_1/c$
Z	1	4
FW	882.71	757.75
a	8.3527(6)	12.8928(6)
b	9.5603(6)	12.0150(6)
c	11.6145(8)	15.5651(7)
α	75.369(2)	90
β	85.004(2)	98.515(2)
γ	70.416(2)	90
V (Å^3)	845.5(1)	2384.6(2)
Density (Mg.m−3)	1.734	2.111
Wavelength (Å)	0.71073	0.71073
μ (mm^{-1})	4.870	7.202
Temperature (K)	100	100
2θ range (°)	2.328 – 28.379	2.150 – 30.545
L.S. parameters, p	205	389
No. of restraints, r	0	0
R/Rw $[I > 2\sigma(I)]$	0.0214/0.0573	0.0185/0.0578
R/Rw (all data) $[I > 2\sigma(I)]$	0.0215/0.0573	0.0252/0.0674
Goof	1.067	1.179

S1.1 Molecular Dynamics (MD) simulations[1]

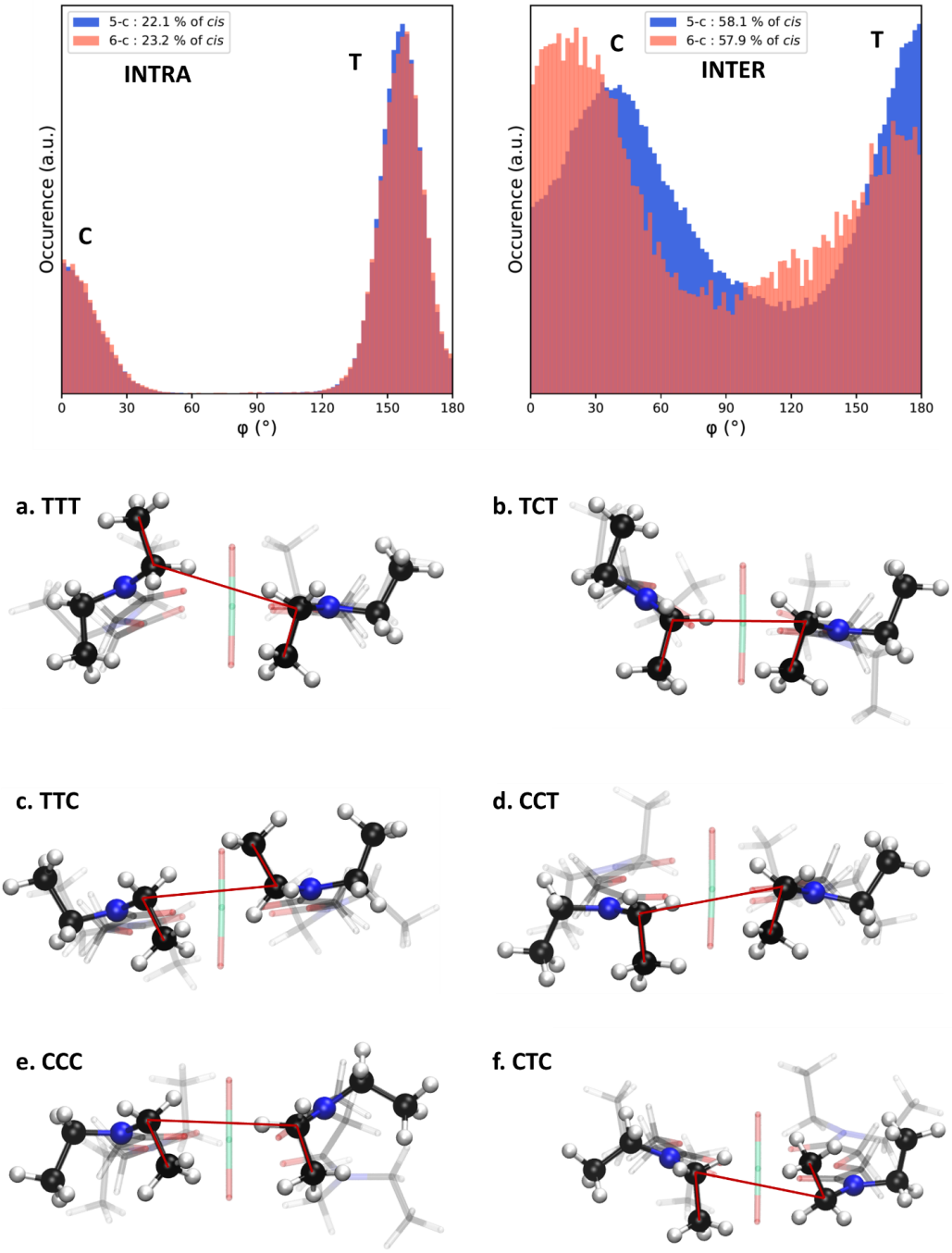

Figure S1: Population in % of each conformer is given for the $[U^{VI}O_2(TEDGA)_2]^{2+}$ structures with the coordination numbers 6 and 5. RDF of the inter and intra dihedral angles (in °) are presented for both structures.

S1.2 DFT optimized structures

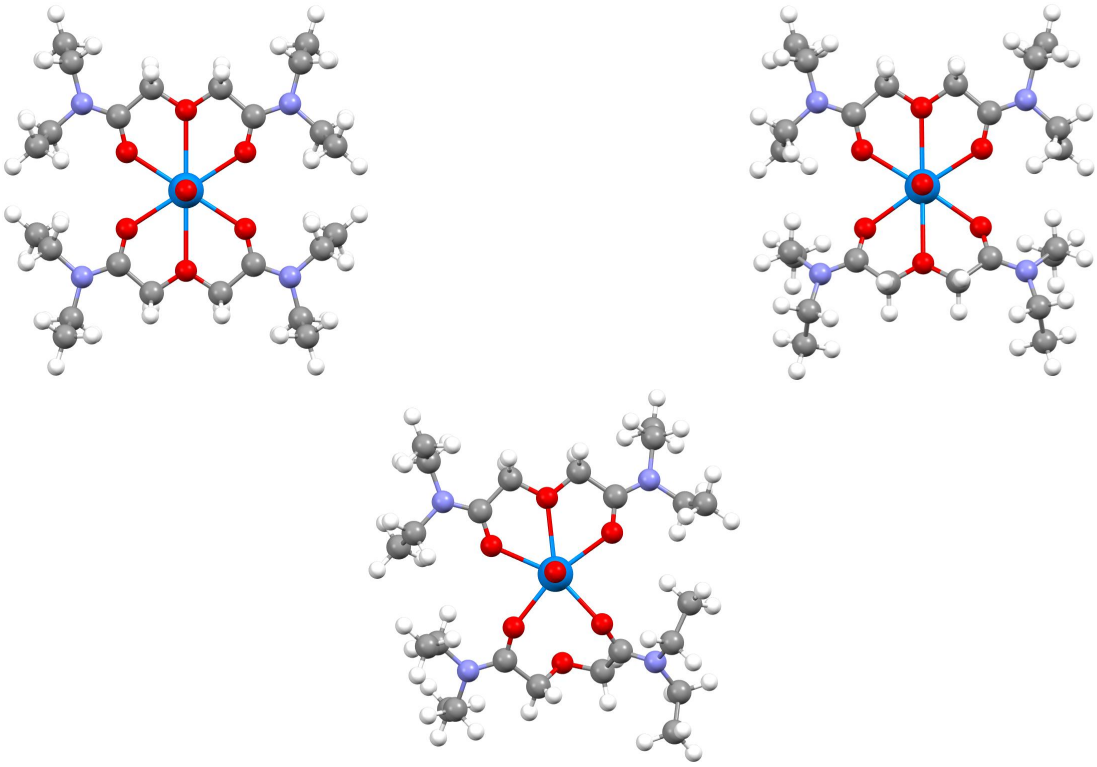

Figure S2: Views of the DFT optimized structure of the $[U^{VI}O_2(TEDGA)_2]^{2+}$ complex in 6c(TTT) (left), 6c(CCC) (center) and 5c(TTT) (right) conformations. Color code: U light blue, O red, N blue, C black, H white. Coordinates are provided in the files u(tedga)2-CN6-TTT.xyz, u(tedga)2-CN6-CCC.xyz u(tedga)2-CN5-TTT.xyz respectively.

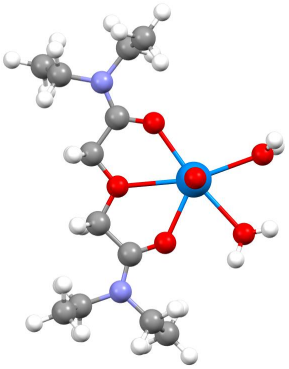

Figure S3: View of the DFT optimized structure of $[U^{VI}O_2(TEDGA)(H_2O)_2]^{2+}$ complex in 5c(T) conformation.Color code: U light blue, O red, N blue, C black, H white. Coordinates of the conformations are provided in the file utedga-2h2o.xyz in SI.

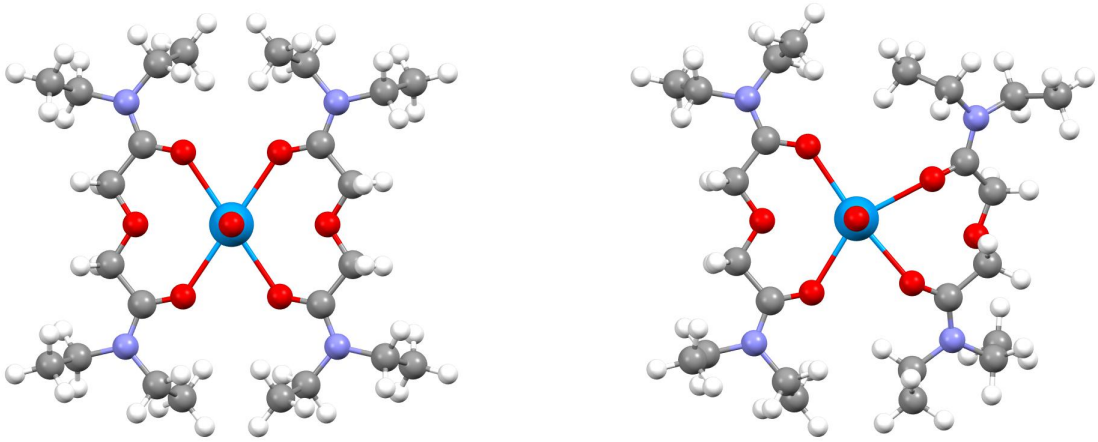

Figure S4: Views of the DFT optimized structure of $[Pa^{V}O_2(TEDGA)_2]^+$ complex with 6c(TTT) (left) and 5c(TTT) (right) conformations. Color code: U light blue, O red, N blue, C black, H white. Coordinates of the conformations are provided in the files patedga-CN6-TTT.xyz and patedga-CN5-TTT.xyz in SI respectively.

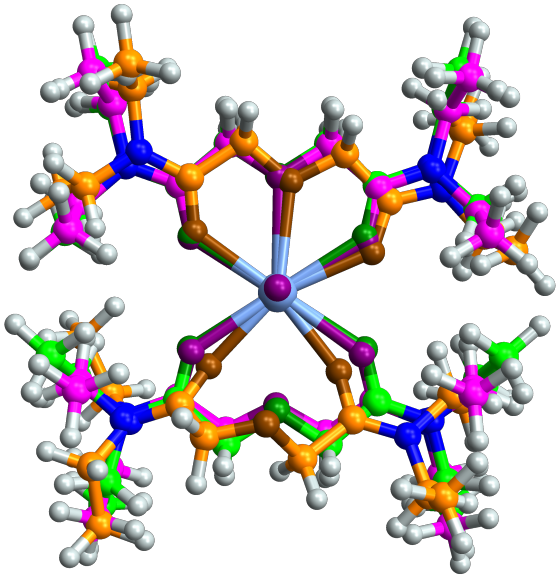

(a) Top view

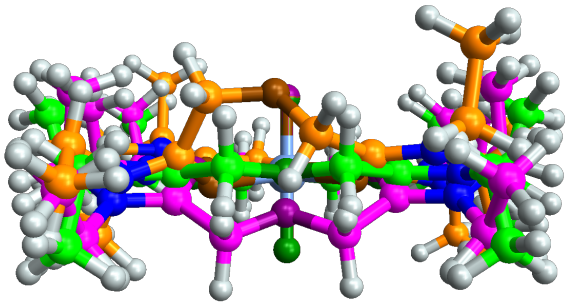

(b) Back view

Figure S5: DFT optimized 6c(TTT), 6c(CCC), and 5c(T) conformations are stacked together to depict the geometrical changes. The backbone carbon and coordinating oxygen atoms of the TEDGA ligands of a specific conformation are represented in the same color as the bright and dark modes. 6c(TTT) is green, 6c(CCC) is magenta, and 5c(T) is orange. The remaining U, N, and H atoms have color codes of light blue, blue, and white, respectively.

S1.3 Analysis of the conformers

In the study of the An^{VI}-DPA complexes, the geometry of the complexes used for pNMR shift calculations were drawn from XRD results.[2] In the present study, the TEDGA is a flexible ligand and structures deduced from solid state owing to X-Ray spectroscopy may not be representative of the complexes' conformation existing in acetonitrile solution. Furthermore

the TEDGA complexes may adopt several conformations in solutions that could be in fast chemical exchange and lead to observed pNMR chemical shifts resulting from an average of these TEDGA conformations.[1] In the TEDGA ligand, carbons 1, 2, 4 and the carbonyl oxygen atom (O1) belong to the amide plane (cf. figure S6). DFT optimization performed on the $[Np^{VI}O_2(TEDGA)_2]^{2+}$ complex exhibits carbonyl oxygens (O1) in first coordination sphere and in the plane perpendicular to the molecular yle cation. A similar DFT optimization performed on the same complex but without the Np^{VI} cation shows that such TEDGA dimer exhibits amid groups of one TEDGA in a plane while the second is non-planar with oxygen atoms O1 outside the plan. It appears that the coordination of the TEDGA to a yle cation requires a ligand deformation forcing the carbonyl oxygen atoms to lay into a common plan perpendicular to the yle oxygens.

The flexible parts of the TEDGA complex mainly arises from the ether oxygen atoms (O2) and the methyl groups in β position of the amide nitrogen (cf. figure S6).

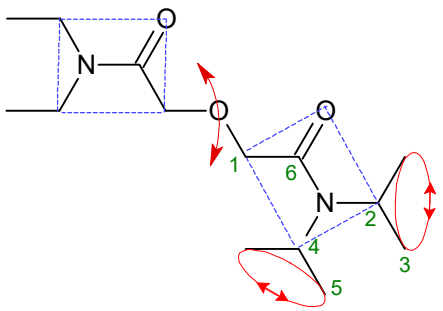

Figure S6: Carbon numbering of the TEDGA molecule. Amide plans are designed with dashed blue lines. To show TEDGA flexibility, atom moves are indicated by red arrows.

Regarding the $[An^{VI}O_2(TEDGA)_2]^{2+}$ complexes, MD simulations showed that the oxygen atoms O1 (1) from the carbonyl are coordinated to the metal center while the oxygen atom O2 of the ethoxy group is not or at least shortly (a few picoseconds), so that the coordination number of the metal center could be 5 or 6.[1] These results differ from XRD data showing complexes with 6 oxygen atoms coordinated to the actinyl in the plan perpendicular to the yl axis. This coordination change of the O2 atom above and below the plane mainly impacts coordinates of the H1 atoms and therefore the associated geometrical factors G through

Eq.(2). However, it has to be pointed out that when one TEDGA is coordinated through two O1 carbonyl atoms, the second TEDGA ligand is coordinated with the three oxygen atoms. Since H1 chemical shift results from an average of H1 positions, in the $[An^{VI}O_2(TEDGA)_2]^{2+}$ complex, we will consider an average of the ^1H coordinates for the coordination numbers 5 and 6 apart. These two corresponding structures will be noted 5c and 6c respectively.

As far as the ethyl chains on the nitrogen atoms, there orientations can be rationalized and depicted in a few conformations owing to two dihedral angles: θ_{intra} defined by the carbons $C3\widehat{C2C}4C5$ belonging to the same amide group and θ_{inter} formed by the carbons $C3\widehat{C2C}2C3$ belonging to the amide groups of different TEDGA inside a $[An^{VI}O_2(TEDGA)_2]^{2+}$ complex. MD simulations point out the occurrence of different conformations at dihedral angles of about 0 and 180° corresponding to eclipsed and staggered conformations respectively. For simplicity of notation, we will note C and T to stand for Cis and $Trans$ conformers when dihedral angle are close to 0 or 180° respectively (See Figure S7).

Since there are two intra and one inter dihedral angles in a $[An^{VI}O_2(TEDGA)_2]^{2+}$ complex, 6 conformers can be assigned : TTT, TTC, TCT, CTC, and CCT and CCC. The first and last letters describe the dihedral angle in a TEDGA ligand (in blue Figure S7) while the letter in the middle describes the dihedral angle formed by ethyl groups arising from two TEDGA ligands (in red Figure S7). Based on this dihedral angle measurements, MD shows the amount of each conformer is independent of the 5c or 6c structures and follow the order: CTC≈CCC<CTT<CCT<TTT<TCT as reported in Table 2. From Radial Distribution Function (RDF) plots of the inter and intra dihedral angles (see Figures S1), it comes out that the fractional populations in close position to Trans, written p_T^{inter} and p_T^{intra}, are about 42 and 77% respectively. The corresponding inter or intra C populations are given by: $p_C^k = 1 - p_T^k$ with $k = inter, intra$. If we consider a random distribution of the ethyl groups of the $[An^{VI}O_2(TEDGA)_2]^{2+}$ complex in these inter and intra positions, we should observe

the probability laws in Eq.(S1):

$$
\begin{aligned}
p_{TTT} &= p_T^{intra} p_T^{inter} p_T^{intra} \\
p_{TTC} &= 2 p_T^{intra} p_T^{inter} p_C^{intra} \\
p_{TCT} &= p_T^{intra} p_C^{inter} p_T^{intra} \\
p_{CTC} &= p_C^{intra} p_T^{inter} p_C^{intra} \\
p_{CCT} &= 2 p_C^{intra} p_C^{inter} p_T^{intra} \\
p_{CCC} &= p_C^{intra} p_C^{inter} p_C^{intra}
\end{aligned}
\tag{S1}
$$

The good agreement reported in Table 2 between populations from MD simulations and calculations obeying simple probability laws, shows that the orientation of the ethyl groups on a TEDGA amide does not affect the ethyl groups orientation on the second TEDGA amide. Such behavior has already been mentioned in an isomeric study with a malonamide ligand (bidendate ligand with 2 amides separated by one sp^3 carbon) where the amide conformation does not affect the second amide.[3]

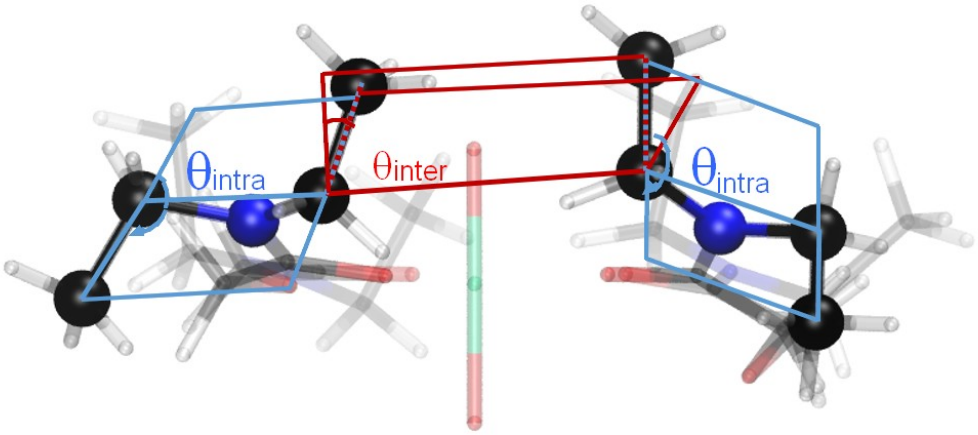

Figure S7: Definition of dihedral angles θ_{intra} (blue) and θ_{inter} (red) in the $[An^{VI}O_2(TEDGA)_2]^{2+}$ complex. The present isomer noted TCT stands for Trans, Cis, Trans for the intra, inter and intra dihedral angles respectively.

From MD results (Table 2), the predominant conformation is the TCT followed by the

TTT while the minority one are the CCC and the CTC conformations whatever the 5c or 6c structure of the $[An^{VI}O_2(TEDGA)_2]^{2+}$ complex. Energy calculations performed by DFT with some of these conformers show that the energy differences between them are small (a few kJ.mol^{-1}) confirming the ethyl chain flexibility of the TEDGA and the difficulty to select privilege conformations. We finally selected the conformer of highest energy CCC (12kJ.mol^{-1} difference) and the most stable TTT one (Table 2) for pNMR shifts calculations and to probe the accuracy or sensitivity of the calculations compared to experimental results.

It has to be mentioned that XRD results present a slight contraction (0.01Å) of the An-O1 distances from U^{VI} to Pu^{VI} complexes (see Table 1). Such accuracy cannot be taken into account here in the selected conformations because the TEDGA flexibility prevents from such detailed analysis. Therefore we considered the U^{VI} as representative for Np^{VI} and Pu^{VI} cations in the DFT optimizations to get the x, y and z coordinates of the $[An^{VI}O_2(TEDGA)_2]^{2+}$ complexes. Regarding the Np^{V} complex, since An-O1 distances are about 0.07Å greater than An^{VI} complexes, x,y and z coordinates are drawn from DFT calculations performed on the $[Pa^{V}O_2(TEDGA)_2]^{+}$ considered as representative of the An^{V} complexes, including the diamagnetic Pa^{V} complex.

DFT energy of the optimized TTT conformer (Table 2) shows that the 5c structure is less stable (8 kJ.mol^{-1} greater) than the 6c one and that this feature is particularly noticeable for the $[An^{V}O_2(TEDGA)_2]^{+}$ complexes since the energy gap is 16 kJ.mol^{-1}. This 8 kJ.mol^{-1} difference between both oxidation states V and VI which represents about 3 times the room temperature energy ($\approx 3k_BT$), exhibits that the 6c structure is more propitious for the An^{V} than the An^{VI} complexes. This is consistent with the Np^{V} carbonyl oxygen O1 distances that are almost 0.1Å longer than in An^{VI} complexes (see Table 1). This leaves more place for the ether oxygen atom O2 to coordinate the metallic center leading to a coordination number of 6.

To rationalize *ab initio* calculations with this flexible TEDGA ligand we limited the num-

ber of conformations to the following selection : Regarding the 1:2 complexes, we consider hereafter the TTT conformer in 5c and 6c structure for both $[An^{VI}O_2(TEDGA)_2]^{2+}$ and $[An^{V}O_2(TEDGA)_2]^{+}$ complexes and the CCC conformer of the 5c $[An^{VI}O_2(TEDGA)_2]^{2+}$ complex which appear the less favorable conformation according to MD and DFT results. (see SI pages S6 and S7 for coordinates)

Regarding the 1:1 complexes from U^{VI} to Pu^{VI}, MD simulations show that two water molecules are in first coordination sphere with the ether and two amide oxygens of the TEDGA coordinated (conformation noted 2W).[1] Aside this 5c structure, another complex with a third water molecule but only two amide oxygens in the first coordination sphere was observed by MD simulations (conformation noted 3W). This complex was found inconsistent with the experimental paramagnetic shifts.[1] Surprisingly, this complex with three water molecules is slightly more stable according to our DFT calculations than the 2W conformation (11kJ/mol difference). Since this energy difference is rather low, only the 2W conformation with Trans ethyl groups is taken into account and noted 5c(T) hereafter. (see SI pages S6 for coordinates) It has to be mentioned that geometry optimization performed by DFT on $[U^{VI}O_2TEDGA(H_2O)_3]^{2+}$ with a coordination number 6 (6c) led to a strong distortion of the first coordination sphere and a loss of one water molecule.

Table S3: Axial geometric factors G_K^{ax} (in $10^{27}\mathrm{m}^{-3}$) of H and C nuclei for different DFT optimized conformations calculated according to Eq.(S2).

		H1	H2	H3	H4	H5
$[U^{VI}O_2(TEDGA)_2]^{2+}$	6c(TTT)	-9.890	-7.200	-3.910	-3.971	-2.492
	6c(CCC)	-7.834	-7.002	-3.631	-3.662	-2.571
	5c(TTT)	-8.541	-7.023	-5.275	-3.950	-1.980
$[U^{VI}O_2(TEDGA)(H_2O)_2]^{2+}$	5c(T)	-10.819	-7.200	-3.878	-4.176	-2.548
$[Pa^{V}O_2(TEDGA)_2]^{+}$	6c(TTT)	-8.902	-6.390	-4.238	-3.559	-2.645
	5c(TTT)	-8.533	-7.269	-5.672	-3.517	-1.9298

		C1	C2	C3	C4	C5	C6
$[U^{VI}O_2(TEDGA)_2]^{2+}$	6c(TTT)	-19.128	-7.5816	-4.930	-4.827	-3.027	-24.385
	6c(CCC)	-16.855	-7.6037	-4.806	-4.630	-3.042	-24.143
	5c(TTT)	-15.886	-7.8442	-5.931	-4.714	-2.574	-24.207
$[U^{VI}O_2(TEDGA)(H_2O)_2]^{2+}$	5c(T)	-	-	-	-	-	-
$[Pa^{V}O_2(TEDGA)_2]^{+}$	6c(TTT)	-17.614	-7.0752	-5.032	-4.481	-3.079	-22.447
	5c(TTT)	-14.567	-7.8636	-6.240	-4.291	-2.456	-21.300

Table S4: Rhombic geometric factors G_K^{rh} (in $10^{27}\mathrm{m}^{-3}$) of H nuclei for different DFT optimized conformations, calculated according to Eq.(S2).

		H1	H2	H3	H4	H5
$[U^{VI}O_2(TEDGA)_2]^{2+}$	6c(TTT)	-13.786	9.036	6.681	-1.263	-0.939
	6c(CCC)	-12.935	8.587	6.441	-1.006	-0.992
	5c(TTT)	-12.470	8.328	7.439	-0.967	-1.063
$[U^{VI}O_2(TEDGA)(H_2O)_2]^{2+}$	5c(T)	14.786	-9.251	-7.303	1.218	0.669
$[Pa^{V}O_2(TEDGA)_2]^{+}$	6c(TTT)	-13.143	7.319	7.467	-1.302	-1.184
	5c(TTT)	-12.663	8.177	8.107	-1.065	-1.185

S2 NMR spectroscopy

S2.1 NMR spectra

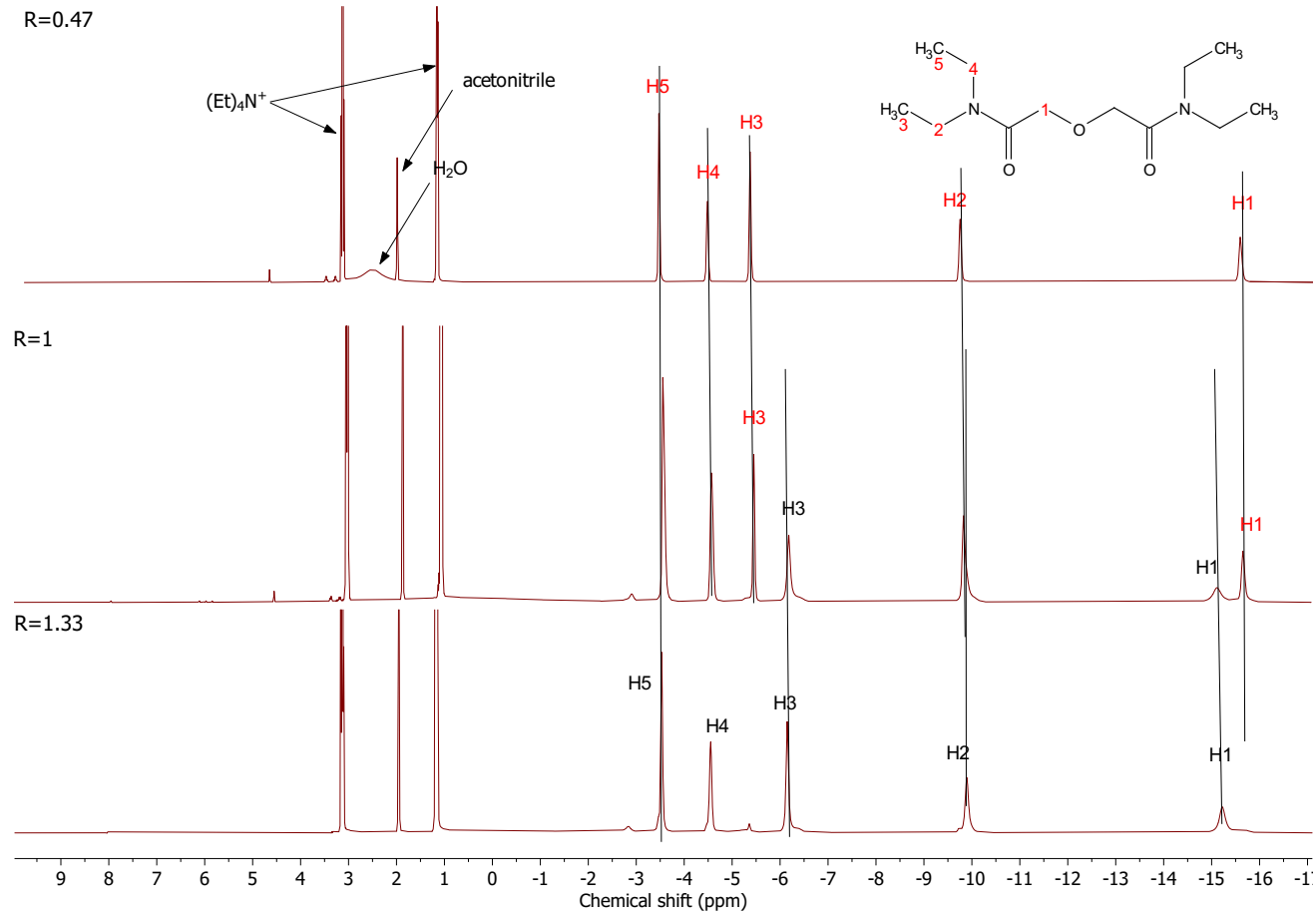

Figure S8: ^{1}H NMR spectra of $[Np^{VI}O_2]^{2+}$ - TEDGA solutions in CD_3CN upon addition of TEDGA ligand at 252 K. Molar ratio R=[Np^{VI}]:[TEDGA] from 1.33 to 0.67 (from bottom to top) with [$NpO_2{}^{2+}$]=25 10^{-3}mol.L^{-1}. ^{1}H assignments in red and black colors correspond to 1:2 and 1:1 complexes respectively.

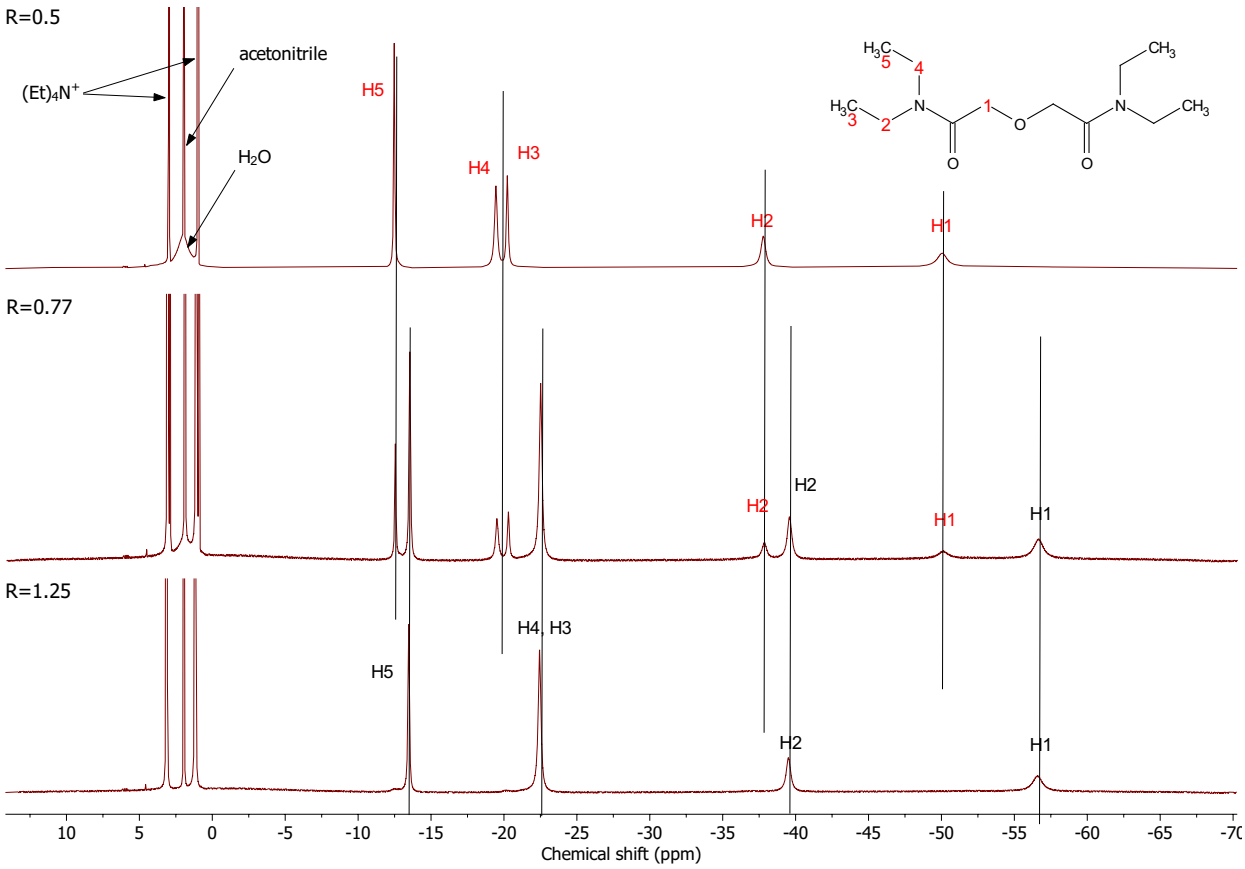

Figure S9: ^{1}H NMR spectra of $[Pu^{VI}O_2]^{2+}$ - TEDGA solutions in CD_3CN upon addition of TEDGA ligand at 252 K. Molar ratio R=$[Pu^{VI}]$:[TEDGA] from 1.25 to 0.5 (bottom to top) with $[PuO_2{}^{2+}]$=25 10^{-3}mol.L^{-1}. ^{1}H assignments in red and black colors correspond to 1:2 and 1:1 complexes respectively.

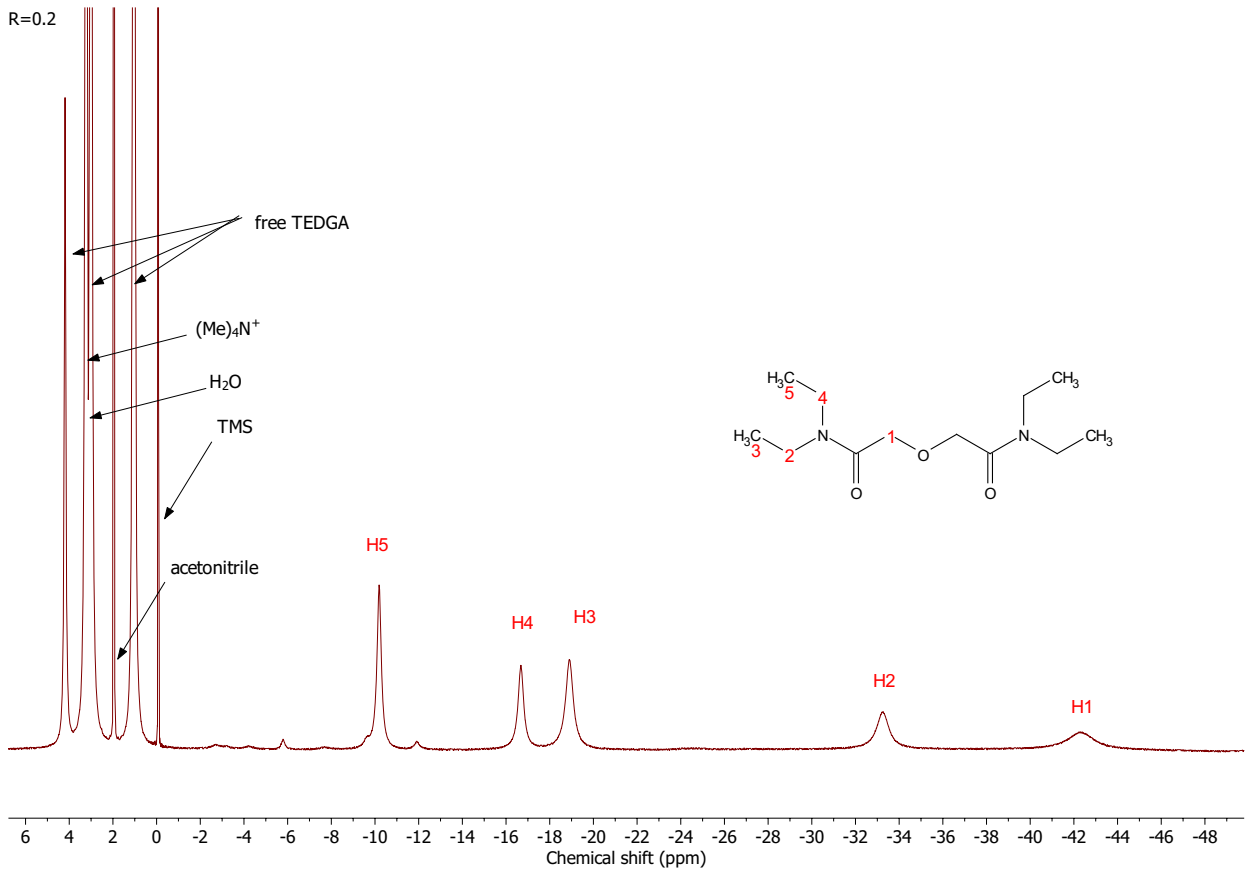

Figure S10: ^{1}H NMR spectrum of the $[Np^{V}(TEDGA)_2]^{+}$ complex. $[Np^{V}O_2]^{+}$ - TEDGA solutions in CD_3CN upon excess addition of TEDGA ligand at 298 K. Molar ratio R = $[Np^{V}]/[TEDGA]$ = 0.2 with $[NpO_2{}^{+}]$ ≈2 0 10^{-3} mol.L^{-1}. The shape of this ^{1}H spectra is similar to those of $[Pu^{VI}(TEDGA)_2]^{2+}$ complex (See top spectra Figure S9).

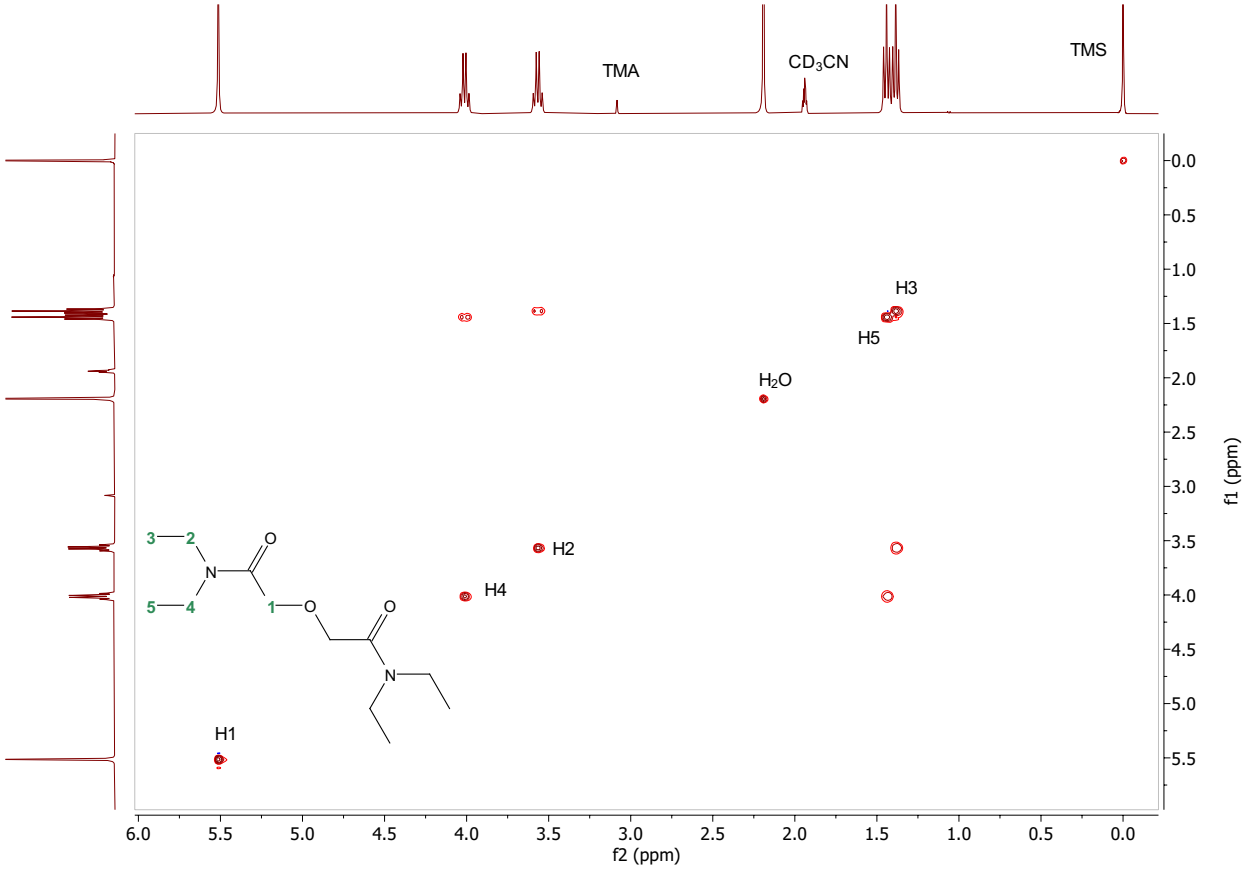

Figure S11: TOCSY spectrum of $[U^{VI}O_2(TEDGA)_2]^{2+} \cdot 2\,(OTf)^- \approx 48$ mmol.L^{-1} in CD_3CN at 298 K (25 °C). TOCSY stands for total correlation spectroscopy. This 2D NMR experiment provides correlations between all the protons that make up a "spin system".

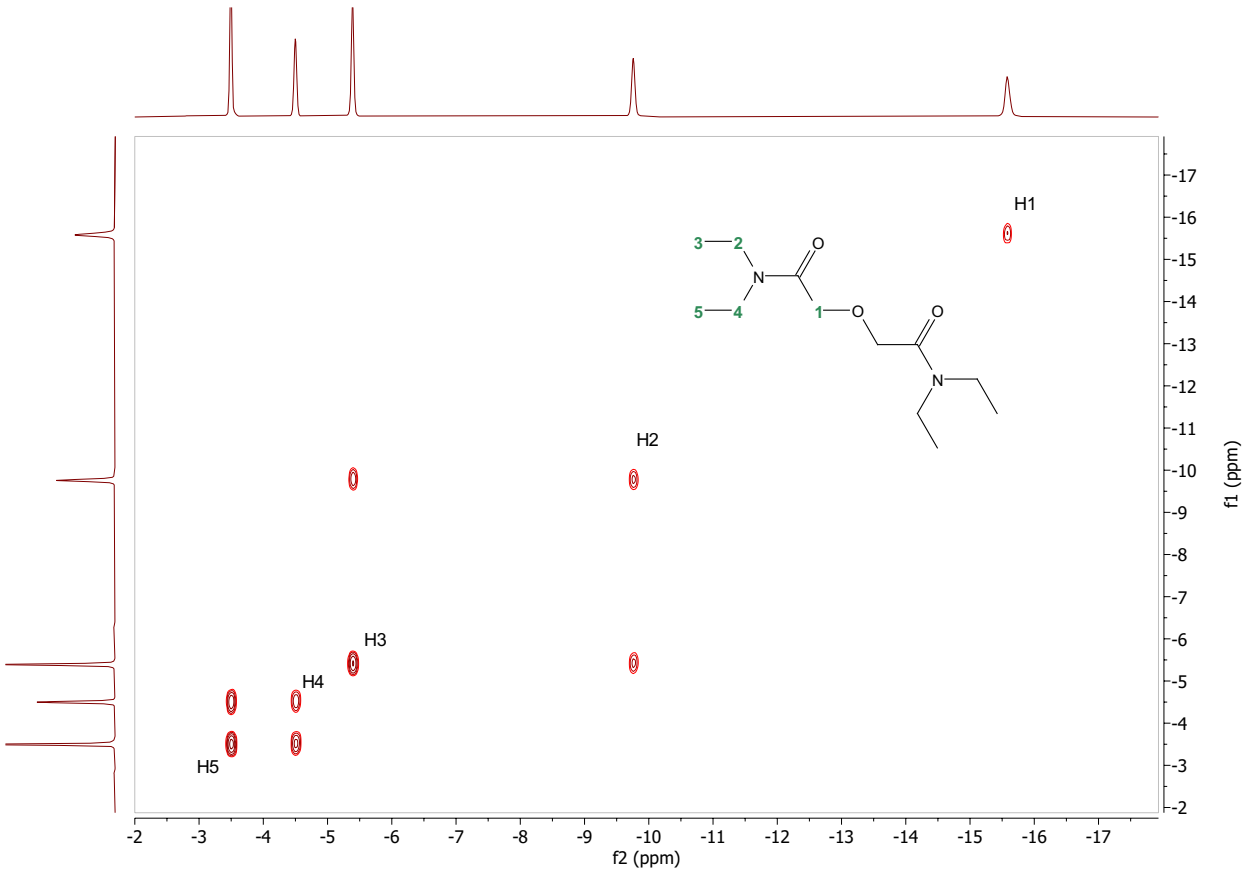

Figure S12: gCOSY spectrum of $[Np^{VI}O_2(TEDGA)_2]^{2+} \cdot 2\,(OTf)^- \approx 34$ mmol.L^{-1} in CD_3CN at 252 K (-21 °C). COSY stands for correlation spectroscopy. This 2D NMR experiment provides correlations between protons over two or three chemical bonds. g means pulsed field gradients are used (in the COSY experiment) to destroy unwanted magnetization.

S2.2 NMR chemical shifts

Table S5: ^{1}H chemical shifts (ppm) of $[An^{VI}O_2(TEDGA)(H_2O)_x]^{2+}$ and $[An^{VI}O_2(TEDGA)_2]^{2+}$ complexes (An = U, Np and Pu) in CD_3CN solution at 298 K. TMS in CD_3CN is used as reference.

		δ_{H_1}	δ_{H_2}	δ_{H_3}	δ_{H_4}	δ_{H_5}
$[An^{VI}O_2(TEDGA)_2]^{2+}$	U^{VI}	5.58	3.568	1.370	4.00	1.425
	Np^{VI}	-12.058	-7.703	-4.197	-3.198	-2.708
	Pu^{VI}	-40.94	-31.32	-15.64	-16.31	-10.12
$[An^{VI}O_2(TEDGA)(H_2O)_x]^{2+}$	U^{VI}	5.722	3.561	1.393	3.999	1.464
	Np^{VI}	-12.04	-7.63	-4.92	-3.14	-2.64
	Pu^{VI}	-46.523	-32.627	-18.039	-18.287	-10.877
$[Np^{V}O_2(TEDGA)_2]^{+}$		-42.196	-33.068	-18.745	-16.548	-10.093

Table S6: ^{13}C chemical shifts (ppm) of $[An^{VI}O_2(TEDGA)_2]^{2+}$ complexes (An = U and Pu) and $[Np^{V}O_2(TEDGA)_2]^{+}$ in CD_3CN solution at 298 K. TMS in CD_3CN is used as reference.

		δ_{C_1}	δ_{C_2}	δ_{C_3}	δ_{C_4}	δ_{C_5}	δ_{C_6}
$[An^{VI}O_2(TEDGA)_2]^{2+}$	U^{VI}	73.271	43.202	112.826	42.231	12.644	175.456
	Np^{VI}	40.54	29.626	5.44	36.234	8.376	133.696

S2.3 Comparison of the ratios

Table S7: Comparison of ^{1}H and ^{13}C pNMR shifts ratios to axial geometric factors G_K^{ax} ratios.

$R_{KK'}$		$\frac{H1}{H5}$	$\frac{H2}{H5}$	$\frac{H3}{H5}$	$\frac{H4}{H5}$	σ_H ‡	$\frac{C1}{C5}$	$\frac{C2}{C5}$	$\frac{C3}{C5}$	$\frac{C4}{C5}$	$\frac{C6}{C5}$	σ_C
$[An^{VI}O_2(TEDGA)_2]^{2+}$												
$\frac{\delta_K^p}{\delta_{K'}^p}$	Np(VI)	4.3	2.7	1.3	1.7		7.7	3.2	1.7	1.4	9.8	
	Pu(VI)	4.0	3.0	1.5	1.8		-	-	-	-	-	
$\frac{G_K^{ax}}{G_{K'}^{ax}}$ †	6c(TTT)	4.0	2.9	1.6	1.6	9%;5%	6.3	2.5	1.6	1.6	8.1	15%
	6c(CCC)	3.0	2.7	1.4	1.4	13%;14% ‖	5.5	2.5	1.6	1.5	7.9	17%
	5c(TTT)	4.3	3.5	2.7	2.0	36%;30%	6.2	3.0	2.3	1.8	9.4	18%
$[An^{VI}O_2(TEDGA)(H_2O)_2]^{2+}$												
$\frac{\delta_K^p}{\delta_{K'}^p}$	Np(VI)	4.3	2.7	1.5	1.7	3%						
	Pu(VI)	4.2	2.9	1.6	1.8	4%						
$\frac{G_K^{ax}}{G_{K'}^{ax}}$ ¶	5c(T)	4.2	2.8	1.5	1.6							
$[Np^{V}O_2(TEDGA)_2]^{+}$												
$\frac{\delta_K^p}{\delta_{K'}^p}$		4.1	3.2	1.7	1.8							
$\frac{G_K^{ax}}{G_{K'}^{ax}}$ §	6c(TTT)	3.4	2.4	1.6	1.3	19%						
	5c(TTT)	4.4	3.8	2.9	1.8	24%						

‡ $\sigma = \frac{1}{N}\sum\left\{\left|\frac{\delta_K^p}{\delta_{K'}^p} - \frac{G_K^{ax}}{G_{K'}^{ax}}\right| / \left(\frac{\delta_K^p}{\delta_{K'}^p}\right)\right\}$; ‖ Np(VI);Pu(VI); † from DFT optimized $[U^{VI}O_2(TEDGA)_2]^{2+}$; ¶ from DFT optimized $[U^{VI}O_2(TEDGA)(H_2O)_2]^{2+}$; § from DFT optimized $[Pa^{V}O_2(TEDGA)_2]^{+}$

Table S8: Calculated ^{1}H and ^{13}C pNMR shifts for the $5f^1$ complexes from magnetic susceptibility tensors collected in Table 4, either using Eq.(3) (ax) or Eq.(2) (ax-rh). Values are in ppm. X_K stands for $^{1}H_K$ or $^{13}C_K$.

conformer	method	$\Delta\chi_{ax}$	$\Delta\chi_{rh}$	X_1	X_2	X_3	X_4	X_5	C_6
				$[Np^{VI}O_2(TEDGA)_2]^{2+}$					
6c(TTT)	ax ^{1}H	3.8	-	-16.72	-12.17	-6.61	-6.71	-4.21	-
	ax ^{13}C	3.8	-	-32.16	-12.75	-8.29	-8.12	-5.09	-41.00
	ax-rh ^{1}H + ^{13}C	3.8	-0.1	-17.22	-11.72	-6.29	-6.73	-4.23	-
				-33.14	-12.41	-7.99	-8.15	-5.13	-41.13
6c(CCC)	ax ^{1}H	4.3		-14.95	-13.37	-6.93	-6.99	-4.91	-
	ax ^{13}C	4.2	-	-31.14	-14.05	-8.88	-8.55	-5.62	-44.61
	ax-rh ^{1}H + ^{13}C	4.0	-0.4	-15.69	-10.82	-5.30	-6.53	-4.63	-
				-32.85	-12.02	-7.30	-8.15	-5.44	-42.46
5c(TTT)	ax ^{1}H	4.0		-14.89	-12.24	-9.19	-6.88	-3.45	-
	ax ^{13}C	4.3	-	-29.82	-14.73	-11.13	-8.85	-4.83	-45.45
	ax-rh ^{1}H + ^{13}C	3.8	-0.6	-17.55	-9.79	-7.06	-6.92	-3.61	-
				-31.95	-11.46	-8.17	-8.16	-4.61	-42.52
				$[Np^{VI}O_2(TEDGA)(H_2O)_2]^{2+}$					
5c(T)	ax ^{1}H	3.7		-17.57	-11.69	-6.30	-6.78	-4.14	-
	ax-rh ^{1}H	3.7	-0.06	-17.82	-11.42	-6.09	-6.77	-4.13	-

Table S9: Calculated ^{1}H pNMR shifts for the $5f^2$ complexes from magnetic susceptibility tensors collected in Table 5, either using Eq.(3) (ax) or Eq.(2) (ax-rh). Values are in ppm.

conformer	method	$\Delta\chi_{ax}$	$\Delta\chi_{rh}$	H_1	H_2	H_3	H_4	H_5
$[Pu^{VI}O_2(TEDGA)_2]^{2+}$								
6c(TTT)	ax ^{1}H	10.8	-	-46.93	-34.17	-18.55	-18.85	-11.82
	ax-rh ^{1}H	10.8	-0.004	-46.91	-34.19	-18.57	-18.84	-11.82
6c(CCC)	ax ^{1}H	12.2	-	-42.24	-37.76	-19.58	-19.75	-13.86
	ax-rh ^{1}H	12.1	-0.76	-46.16	-34.47	-17.21	-19.88	-14.05
5c(TTT)	ax ^{1}H	11.2	-	-42.05	-34.57	-25.96	-19.44	-9.75
	ax-rh ^{1}H	11.1	-0.99	-47.15	-30.68	-22.53	-19.72	-10.14
$[Pu^{VI}O_2(TEDGA)(H_2O)_2]^{2+}$								
5c(T)	ax ^{1}H	11.2	-	-53.38	-35.53	-19.14	-20.61	-12.57
	ax-rh ^{1}H	11.3	-0.16	-52.62	-36.34	-19.73	-20.62	-12.59
$[Np^{V}O_2(TEDGA)_2]^{+}$								
6c(TTT)	ax ^{1}H	12.2	-	-47.87	-34.36	-22.79	-19.14	-14.23
	ax-rh ^{1}H	12.2	-0.004	-47.89	-34.35	-22.78	-19.14	-14.23
5c(TTT)	ax ^{1}H	11.5	-	-43.29	-36.88	-28.78	-17.84	-9.79
	ax-rh ^{1}H	11.5	-0.1	-48.84	-33.01	-24.98	-18.25	-10.28

S2.4 Temperature dependence of the AIS

Table S10: ^{1}H chemical shifts (ppm) of $U^{VI}(TEDGA)_2(OTf)_2$ in CD_3CN with temperature T (°C and K). TMS in CD_3CN is used as reference.

T		H1	H4	H2	H5	H3
°C	K					
62.51	335.5	5.571	4.032	3.602	1.450	1.398
57.13	330.1	5.570	4.028	3.597	1.447	1.395
51.75	324.8	5.568	4.024	3.593	1.444	1.391
46.37	319.4	5.566	4.019	3.588	1.441	1.387
41.00	314.0	5.564	4.015	3.583	1.437	1.383
35.62	308.6	5.562	4.010	3.577	1.433	1.379
30.24	303.2	5.559	4.004	3.572	1.429	1.374
25.00	298.0	5.558	4.000	3.568	1.425	1.370
18.56	291.6	5.556	3.995	3.562	1.422	1.366
12.88	285.9	5.554	3.990	3.556	1.418	1.361
7.21	280.2	5.552	3.985	3.551	1.413	1.356
1.54	274.5	5.550	3.980	3.546	1.409	1.352
-4.13	268.9	5.547	3.975	3.540	1.405	1.347
-9.80	263.2	5.545	3.970	3.535	1.401	1.343
-15.47	257.5	5.543	3.964	3.529	1.397	1.338
-21.14	251.9	5.541	3.961	3.525	1.394	1.335
-26.81	246.2	5.539	3.957	3.521	1.391	1.331
-32.48	240.5	5.537	3.951	3.515	1.386	1.325
-38.15	234.9	5.535	3.944	3.508	1.380	1.319
-43.82	229.2	5.533	3.939	3.503	1.376	1.315
-49.49	223.5	5.531	3.934	3.498	1.372	1.310

Table S11: ^{13}C chemical shifts (ppm) of $U^{VI}(TEDGA)_2(OTf)_2$ in CD_3CN with temperature T (°C and K). TMS in CD_3CN is used as reference.

T		C6	C1	C2	C4	C3	C5
°C	K						
62.51	335.5	175.907	73.582	43.630	42.728	13.171	12.913
57.13	330.1	175.847	73.540	43.574	42.660	13.126	12.879
51.75	324.8	175.786	73.498	43.517	42.591	13.080	12.845
46.37	319.4	175.718	73.453	43.456	42.523	13.031	12.803
41.00	314.0	175.649	73.407	43.395	42.455	12.981	12.761
35.62	308.6	175.589	73.366	43.335	42.383	12.932	12.727
30.24	303.2	175.528	73.324	43.274	42.310	12.883	12.693
25.00	298.0	175.456	73.271	43.202	42.231	12.826	12.644
18.56	291.6	175.384	73.217	43.130	42.151	12.769	12.595
12.88	285.9	175.320	73.176	43.066	42.075	12.720	12.553
7.21	280.2	175.255	73.134	43.001	41.999	12.670	12.511
1.54	274.5	175.194	73.093	42.933	41.924	12.617	12.466
-4.13	268.9	175.133	73.051	42.864	41.848	12.564	12.420
-9.80	263.2	175.069	73.006	42.800	41.776	12.511	12.379
-15.47	257.5	175.004	72.960	42.735	41.704	12.458	12.337
-21.14	251.9	174.944	72.918	42.663	41.628	12.401	12.292
-26.81	246.2	174.883	72.876	42.591	41.552	12.344	12.246
-32.48	240.5	174.822	72.831	42.519	41.469	12.284	12.197
-38.15	234.9	174.761	72.785	42.447	41.385	12.223	12.147
-43.82	229.2	174.701	72.747	42.379	41.309	12.166	12.098
-49.49	223.5	174.640	72.709	42.310	41.233	12.109	12.048

Table S12: ^{1}H chemical shifts (ppm) of $Np^{VI}(TEDGA)_2(OTf)_2$ in CD_3CN with temperature T (°C and K). TMS in CD_3CN is used as reference.

T		H5	H4	H3	H2	H1
°C	K					
67.89	338.0	-2.142	-2.25	-3.361	-6.224	-9.587
62.51	335.5	-2.204	-2.365	-3.453	-6.391	-9.860
57.13	330.1	-2.266	-2.48	-3.545	-6.557	-10.133
51.75	324.8	-2.328	-2.584	-3.637	-6.721	-10.409
46.37	319.4	-2.39	-2.687	-3.728	-6.885	-10.685
41.00	314.0	-2.478	-2.827	-3.857	-7.109	-11.055
35.62	308.6	-2.548	-2.939	-3.96	-7.286	-11.353
30.24	303.2	-2.636	-3.08	-4.088	-7.513	-11.735
25.00	298.0	-2.708	-3.198	-4.197	-7.703	-12.058
18.56	291.6	-2.814	-3.372	-4.356	-7.974	-12.515
12.88	285.9	-2.911	-3.525	-4.499	-8.223	-12.936
7.21	280.2	-2.997	-3.666	-4.629	-8.443	-13.308
1.54	274.5	-3.114	-3.854	-4.804	-8.742	-13.814
-4.13	268.9	-3.221	-4.030	-4.968	-9.020	-14.285
-9.80	263.2	-3.328	-4.205	-5.132	-9.297	-14.756
-15.47	257.5	-3.445	-4.394	-5.309	-9.594	-15.264
-21.14	251.9	-3.561	-4.583	-5.486	-9.891	-15.772
-26.81	246.2	-3.666	-4.757	-5.649	-10.17	-16.258
-32.48	240.5	-3.812	-4.994	-5.873	-10.538	-16.885
-38.15	234.9	-3.95	-5.22	-6.086	-10.891	-17.494
-43.82	229.2	-4.084	-5.439	-6.294	-11.235	-18.09
-49.49	223.5	-4.227	-5.675	-6.516	-11.603	-18.728

Table S13: ^{13}C chemical shifts (ppm) of $Np^{VI}(TEDGA)_2(OTf)_2$ in CD_3CN with temperature T (°C and K). TMS in CD_3CN is used as reference.

T		C6	C1	C4	C2	C5	C3
°C	K						
67.89	338.0	138.832	45.178	37.469	31.469	9.272	6.662
62.51	335.5	138.301	44.723	37.405	31.420	9.170	6.533
57.13	330.1	137.770	44.268	37.341	31.371	9.067	6.404
51.75	324.8	137.110	43.644	37.163	31.132	8.953	6.222
46.37	319.4	136.450	43.020	36.985	30.893	8.839	6.040
41.00	314.0	135.896	42.424	36.818	30.574	8.733	5.880
35.62	308.6	135.180	41.863	36.636	30.248	8.627	5.752
30.24	303.2	134.455	41.165	36.431	29.937	8.498	5.650
25.00	298.0	133.696	40.540	36.234	29.626	8.376	5.440
18.56	291.6	132.801	39.610	36.100	29.239	8.217	5.200
12.88	285.9	131.959	38.870	35.818	28.879	8.077	4.998
7.21	280.2	131.117	38.130	35.536	28.518	7.936	4.796
1.54	274.5	130.195	37.292	35.297	28.128	7.788	4.576
-4.13	268.9	129.273	36.454	35.058	27.737	7.640	4.356
-9.80	263.2	128.242	35.500	34.785	27.305	7.481	4.098
-15.47	257.5	127.300	34.534	34.534	26.902	7.300	3.863
-21.14	251.9	126.230	33.680	34.254	26.455	7.102	3.627
-26.81	246.2	125.200	32.440	33.988	25.689	6.988	3.339
-32.48	240.5	124.040	31.500	33.677	25.529	6.783	3.051
-38.15	234.9	122.870	30.453	33.381	25.059	6.670	2.755
-43.82	229.2	121.670	29.300	33.063	24.528	6.434	2.550
-49.49	223.5	120.400	28.090	32.750	24.000	6.270	2.150

Table S14: ^{1}H chemical shifts (ppm) of $Pu^{VI}(TEDGA)_2(OTf)_2$ in CD_3CN with temperature T (°C and K). TMS in CD_3CN is used as reference.

T		H5	H4	H3	H2	H1
°C	K					
62.51	335.5	-8.73	-13.91	-13.42	-27.17	-35.15
57.13	330.1	-8.925	-14.245	-13.71	-27.73	-35.95
51.75	324.8	-9.12	-14.58	-14	-28.29	-36.74
46.37	319.4	-9.19	-14.75	-14.21	-28.69	-37.30
41.00	314.0	-9.41	-15.13	-14.52	-29.28	-38.13
35.62	308.6	-9.63	-15.51	-14.87	-29.95	-39.04
30.24	303.2	-9.87	-15.91	-15.25	-30.6	-39.99
25.00	298.0	-10.12	-16.31	-15.64	-31.32	-40.94
18.56	291.6	-10.36	-16.73	-16.04	-32	-41.97
12.88	285.9	-10.61	-17.16	-16.45	-32.74	-42.97
7.21	280.2	-10.87	-17.61	-16.89	-33.51	-44.04
1.54	274.5	-11.15	-18.09	-17.36	-34.3	-45.18
-4.13	268.9	-11.43	-18.58	-17.81	-35.11	-46.30
-9.80	263.2	-11.74	-19.08	-18.33	-35.99	-47.55
-15.47	257.5	-12.04	-19.63	-18.83	-36.9	-48.83
-21.14	251.9	-12.37	-20.16	-19.36	-37.84	-50.16
-26.81	246.2	-12.7	-20.76	-19.95	-38.8	-51.53
-32.48	240.5	-13.06	-21.31	-20.53	-39.84	-53.00
-38.15	234.9	-13.41	-22	-21.17	-40.88	-54.51
-43.82	229.2	-13.81	-22.66	-21.89	-41.97	-56.15
-49.49	223.5	-14.25	-23.44	-22.63	-43.34	-58.00

Table S15: ^{1}H chemical shifts (ppm) of $Np^V(TEDGA)_2(OTf)$ in CD_3CN with temperature T (°C and K). TMS in CD_3CN is used as reference.

T		H5	H4	H3	H2	H1
°C	K					
67.89	338.0	-8.266	-13.557	-15.641	-28.183	-34.978
62.51	335.5	-8.43	-13.924	-16.021	-28.652	-35.747
57.13	330.1	-8.693	-14.292	-16.413	-29.302	-36.685
51.75	324.8	-8.914	-14.606	-16.757	-29.842	-37.56
46.37	319.4	-9.123	-14.939	-17.132	-30.432	-38.375
41.00	314.0	-9.341	-15.285	-17.482	-30.993	-39.084
35.62	308.6	-9.63	-15.774	-17.976	-31.796	-40.255
30.24	303.2	-9.853	-16.165	-18.374	-32.432	-41.281
25.00	298.0	-10.09	-16.548	-18.745	-33.068	-42.196
18.56	291.6	-10.41	-17.103	-19.309	-33.964	-43.324
12.88	285.9	-10.66	-17.511	-19.744	-34.646	-44.345
7.21	280.2	-10.97	-18.037	-20.271	-35.507	-45.514
1.54	274.5	-11.21	-18.456	-20.705	-36.188	-46.622
-4.13	268.9	-11.56	-19.047	-21.294	-37.214	-48.001
-9.80	263.2	-11.84	-19.515	-21.791	-37.963	-49.088
-15.47	257.5	-12.18	-20.104	-22.385	-38.901	-50.494
-21.14	251.9	-12.48	-20.627	-22.909	-39.834	-51.666
-26.81	246.2	-12.89	-21.339	-23.657	-40.011	-53.479
-32.48	240.5	-13.21	-21.893	-24.214	-41.862	-54.676
-38.15	234.9	-13.6	-22.563	-24.90	-43.005	-56.352
-43.82	229.2	-13.96	-23.196	-25.542	-44.029	-58.023
-49.49	223.5	-14.40	-23.962	-26.357	-45.324	-59.704

Table S16: ^{1}H chemical shifts (ppm) of $U^{VI}(TEDGA)(H_2O)_x(OTf)_2$ in CD_3CN with temperature T (°C and K). TMS in CD_3CN is used as reference.

T		H1	H4	H2	H5	H3	H_2O
°C	K						
62.51	335.5	5.726	4.049	3.597	1.496	1.424	2.694
51.75	324.8	5.725	4.037	3.588	1.488	1.416	2.874
41	314.0	5.722	4.019	3.575	1.476	1.404	3.009
30.24	303.2	5.722	4.006	3.566	1.468	1.397	3.221
25.00	298.0	5.722	3.999	3.561	1.464	1.393	3.359
18.56	291.6	5.722	3.992	3.556	1.459	1.388	3.496
7.21	280.2	5.726	3.983	3.551	1.455	1.384	3.752
-4.13	268.9	5.722	3.964	3.538	1.443	1.371	4.069
-15.47	257.5	5.721	3.949	3.527	1.434	1.362	4.432
-26.81	246.2	5.719	3.934	3.518	1.425	1.354	4.812
-38.15	234.9	5.721	3.923	3.512	1.420	1.348	5.199
-49.49	223.5	5.714	3.903	3.496	1.406	1.334	5.49

Table S17: ^{1}H chemical shifts (ppm) of $Np^{VI}(TEDGA)(H_2O)_x(OTf)_2$ in CD_3CN with temperature T (°C and K). TMS in CD_3CN is used as reference.

T		H1	H2	H3	H4	H5
°C	K					
25.00	298.0	-12.040	-7.630	-4.92	-3.140	-2.640
-21.14	251.9	-15.550	-10.040	-6.220	-4.620	-3.56

Table S18: ^{1}H chemical shifts (ppm) of $Pu^{VI}(TEDGA)(H_2O)_x(OTf)_2$ in CD_3CN with temperature T (°C and K respectively). TMS in CD_3CN is used as reference.

T		H5	H4	H3	H2	H1	H_2O
°C	K						
62.51	335.5	-9.264	-15.284	-15.676	-28.280	-39.779	0.93
57.13	330.1	-9.469	-15.625	-16.008	-28.817	-40.588	0.84
51.75	324.8	-9.685	-15.997	-16.351	-29.398	-41.413	0.66
46.37	319.4	-9.893	-16.352	-16.699	-29.969	-42.335	0.5
41.00	314.0	-10.121	-16.753	-17.067	-30.601	-43.283	0.6
35.62	308.6	-10.343	-17.128	-17.412	-31.147	-44.106	1.2
30.24	303.2	-10.605	-17.599	-17.834	-31.944	-45.371	1
25.00	298.0	-10.877	-18.287	-18.039	-32.627	-46.523	1.7
18.56	291.6	-11.145	-18.712	-18.712	-33.404	-47.750	2
12.88	285.9	-11.400	-19.138	-19.138	-34.082	-48.810	2.2
7.21	280.2	-11.703	-19.624	-19.624	-35.045	-50.250	2.1
1.54	274.5	-11.980	-20.079	-20.079	-35.700	-51.314	2.7
-4.13	268.9	-12.316	-20.625	-20.625	-36.843	-52.657	2.8
-9.80	263.2	-12.627	-21.097	-21.097	-37.645	-53.939	2.6
-15.47	257.5	-13.016	-21.748	-21.748	-38.643	-55.517	2.5
-21.14	251.9	-13.470	-22.450	-22.450	-39.510	-56.580	-
-26.81	246.2	-13.768	-22.925	-22.925	-40.565	-58.389	3
-32.48	240.5	-	-	-	-	-	-
-38.15	234.9	-14.639	-24.237	-24.237	-42.730	-61.692	2.8
-43.82	229.2	-	-	-	-	-	-
-49.49	223.5	-15.681	-25.837	-25.837	-45.392	-65.772	5

S3 Magnetic susceptibility tensor χ

S3.1 Magnetic susceptibility tensor $\boldsymbol{\chi}$ deduced fom AIS

The pseudo-contact shift of a nucleus K δ_K^{pc} is expressed in terms of the axial and rhombic components of the $\boldsymbol{\chi}$ tensor according to[4]

$$\delta_K^{pc} = \frac{10^6}{12\pi N_A}(\Delta\chi_{ax}G_K^{ax} + \Delta\chi_{rh}G_K^{rh}) \tag{2}$$

where δ_K^{pc} is expressed in ppm, N_A is Avogadro constant, and $\mathbf{r}_K$ is the position of nucleus K $\mathbf{r}_K$, defining the axial and rhombic geometrical factors G_K^{ax} and G_K^{rh} as

$$G_K^{ax} = \frac{3z_K^2}{r_K^5} - \frac{1}{r_K^3} \quad \text{and} \quad G_K^{rh} = \frac{3}{2}\frac{x_K^2 - y_K^2}{r_K^5} \tag{S2}$$

In the present study, the PAF is foreseen from the symmetry of the complexes: the axial direction z is along the yle bond, and one equatorial along the x and the other one along the y. Those axes are chosen in order to fulfill Bertini's convention. With $\Delta\chi_{rh}$ opposite in sign to $\Delta\chi_{ax}$.[5] In case where this condition is not fulfilled, one should permute the x and y axes. This convention is further applied to *ab intio* calculations.

This is a linear set of equations of the two unknowns $\Delta\chi_{ax}$ and $\Delta\chi_{rh}$ in terms of the N G_K^{ax} and G_K^{rh} determined for a given structural geometry. Written in a matrix form we have

$$\begin{pmatrix} \delta_1^{pc} \\ \vdots \\ \delta_N^{pc} \end{pmatrix} = \frac{10^6}{12\pi \mathrm{N_A}} \begin{pmatrix} G_1^{ax} & G_1^{rh} \\ \vdots & \vdots \\ G_N^{ax} & G_N^{rh} \end{pmatrix} \begin{pmatrix} \Delta\chi_{ax} \\ \Delta\chi_{rh} \end{pmatrix} \tag{S3}$$

or

$$\overrightarrow{D} = \mathbf{G}.\overrightarrow{C} \tag{S4}$$

with $\overrightarrow{D}$ the vector representing the N experimental AIS (columns of δ_K^{pc}) multiplied by $12\pi \mathrm{N_A}.10^{-6}$, $\overrightarrow{C}$ is the vector formed by the axial and rhombic components of the $\boldsymbol{\chi}$ tensor

and **G** is the matrix made of axial and rhombic geometrical factors for the different active nuclei (G_K^{ax}, G_K^{rh}).

We solved Eq.(2) using two methods: i) The direct method consists in applying the least squares regression model in the matrix form: $\overrightarrow{C}$=$(\mathbf{G}^t\ \mathbf{G})^{-1}$. $(\mathbf{G}^t\overrightarrow{D})$. ($\mathbf{G}^t$ stands for the transpose of the **G** matrix).

ii) An iterative least square method written in Python[6] looking for a minimum value of the quality factor Q_{pc}

$$Q_{pc} = \sqrt{\frac{\sum_K (\delta_K^{pc,exp} - \delta_K^{pc,calc})^2}{\sum_K (\delta_K^{pc,exp})^2}} \tag{S5}$$

closely related to the rmsd (Root-Mean-Square Deviation) value.[7].

Table S19 presents the magnetic susceptibility components determined with all the MD conformations of each conformers with Eqs.(3) (ax) and (2) (ax-rh), with the Q_{pc} factor associated. The addition of the rhombic component improves the fit, but it is because the experimental AIS represents the whole conformation and not only one conformer. We can see that all conformers have a similar $\boldsymbol{\chi}$ component for the same cation, contrary to what was determined with the DFT optimized conformations (Tables 4 and 5), showing the importance of taking into account all conformations of each conformer. This is in agreement with the SO-CASPT2 values, which remain similar for the different conformers.

The MD mix values, corresponding to the magnetic susceptibility components determined with the MD simulation proportion of each conformer (Table 2) and the optimal values for the optimal proportion of the 5c and 6c structures were determined in our previous paper[1]. The $\Delta\chi_{ax}$ values are 12.3 and 12.9 10^{-8}m^3.mol^{-1}for the Pu^{VI} and Np^{V} complexes, respectively, which are close to those determined by SO-CASPT2, with 13.3 and 13.9 10^{-8}m^3.mol^{-1} for the Pu^{VI} and Np^{V} 6c(TTT) complexes, respectively. For these $5f^2$ cations, less than 10% of difference is observed. The CASPT2 values are more dependent of the conformer for the Np^{VI} cation, but the $\Delta\chi_{ax}$ from MD (4.3 10^{-8}m^3.mol^{-1}) remains at the same order of

magnitude.

Table S19: Magnetic susceptibility tensor at 298 K (in 10^{-8}m^3.mol^{-1}) for different conformers, deduced from the fit of the ^{1}H AIS with the MD geometric factors. The fit is performed either using Eq.(3) (ax) or Eq.(2) (ax-rh). Q_{pc} (in %) characterizes the standard deviation of the fitting procedure (see Eq.(S5)).

	5c					6c				
	ax		ax-rh			ax		ax-rh		
Np^{VI}	$\Delta\chi_{ax}$	Q_{pc}	$\Delta\chi_{ax}$	$\Delta\chi_{rh}$	Q_{pc}	$\Delta\chi_{ax}$	Q_{pc}	$\Delta\chi_{ax}$	$\Delta\chi_{rh}$	Q_{pc}
(TTT)	4.3	7.3	4.3	-0.2	4.8	4.2	6.6	4.3	-0.2	1.8
(TCT)	4.4	6.5	4.4	-0.1	5.2	4.1	8.4	4.3	-0.2	4.8
(TTC)	4.3	8.2	4.2	-0.2	6.2	4.1	5.7	4.3	-0.2	1.9
(CCT)	4.4	6.5	4.4	-0.1	5.4	4.1	8.6	4.3	-0.2	5.2
(CCC)	4.4	5.4	4.4	-0.1	4.5	4.1	9.3	4.3	-0.2	6.3
(CTC)	4.3	9.2	4.2	-0.1	8.0	4.1	6.7	4.2	-0.2	1.4
MD mix			4.3	-0.1	3.4			4.3	-0.2	3.5
Optimal	for 67% of 5c and 33% of 6c:							4.3	0	2.4
	5c					6c				
	ax		ax-rh			ax		ax-rh		
Pu^{VI}	$\Delta\chi_{ax}$	Q_{pc}	$\Delta\chi_{ax}$	$\Delta\chi_{rh}$	Q_{pc}	$\Delta\chi_{ax}$	Q_{pc}	$\Delta\chi_{ax}$	$\Delta\chi_{rh}$	Q_{pc}
(TTT)	12.1	4.4	12.1	-0.1	4.3	11.5	12.8	12.2	-1.2	2.8
(TCT)	12.4	5.6	12.5	-0.2	5.1	11.5	14.2	12.2	-1.2	5.6
(TTC)	12.0	5.8	12.1	-0.1	5.7	11.5	11.9	12.2	-1.1	2.8
(CCT)	12.4	6.0	12.5	-0.2	5.4	11.5	14.3	12.2	-1.2	6.1
(CCC)	12.3	5.0	12.4	-0.3	3.8	11.5	14.9	12.3	-1.2	7.3
(CTC)	12.0	7.8	12.0	-0.1	7.6	11.4	12.8	12.1	-1.2	1.6
MD mix			12.3	-0.2	2.6			12.2	-1.2	4.3
Optimal	for 82% of 5c and 18% of 6c:							12.3	-0.4	2.4
	5c					6c				
	ax		ax-rh			ax		ax-rh		
Np^{V}	$\Delta\chi_{ax}$	Q_{pc}	$\Delta\chi_{ax}$	$\Delta\chi_{rh}$	Q_{pc}	$\Delta\chi_{ax}$	Q_{pc}	$\Delta\chi_{ax}$	$\Delta\chi_{rh}$	Q_{pc}
(TTT)	12.6	7.9	12.7	-0.3	7.3	12.0	14.9	12.8	-1.5	1.8
(TCT)	12.9	6.2	13.1	-0.5	4.0	12.0	15.7	12.9	-1.5	2.6
(TTC)	12.5	9.2	12.6	-0.3	8.7	12.0	14.1	12.8	-1.4	2.3
(CCT)	12.9	6.9	13.1	-0.5	4.6	12.0	15.8	12.9	-1.5	3.4
(CCC)	12.8	7.9	13.0	-0.6	5.6	12.0	16.2	12.9	-1.5	5.0
(CTC)	12.4	11.2	12.6	-0.4	10.5	11.9	15.5	12.7	-1.5	3.7
MD mix			12.9	-0.4	4.3			12.9	-1.5	1.8
Optimal	for 20% of 5c and 80% of 6c:							12.9	-1.3	1.6

S3.2 Modelling the AIS

Two Kramers Doublets (KDs) model for $5f^1$ actinyl complexes

The axial magnetic susceptibility can be expressed in terms of the representation matrices of the magnetic moment operator $\hat{\mathbf{M}} = -\mu_B(\hat{\mathbf{L}} + g_e\hat{\mathbf{S}})$ where $\mathbf{L}$ and $\mathbf{S}$ denote the orbital and spin moment operators respectively and μ_B Bohr magneton[2]

$$\Delta\chi_{ax} = N_A\mu_0\mu_B^2\frac{1}{Q_0}\sum_{n=1,2} e^{-\frac{E_n}{kT}}\left[\frac{\Delta M_{nn}^2}{kT} + 2\sum_{m\neq n}\frac{\Delta M_{nm}^2}{E_m - E_n}\right] \tag{S6}$$

where n, m count the two KDs, $\Delta M_{nm}^2 = \|\mathbf{M}_{z,nm}\|^2 - \frac{1}{2}\left(\|\mathbf{M}_{x,nm}\|^2 + \|\mathbf{M}_{y,nm}\|^2\right)$, $\|\|$ represents the norm of the matrix, and $\mathbf{M}_{z,nm}$ is the matrix representation of $\hat{\mathbf{M}}$ in the block nm. Q_0 is the partition function, μ_0 the magnetic permeability and k the Boltzmann constant. In the case of axial symmetry $\|\mathbf{M}_{x,nm}\|^2 = \|\mathbf{M}_{y,nm}\|^2 = \|\mathbf{M}_{\perp,nm}\|^2$.

In the $[Np^{VI}O_2]^{2+}$ complexes, the two lowest energetically well isolated KDs, KD1 and KD2 separated by energy Δ, are mostly responsible for the magnetic behavior. As shown for the $[Np^{VI}O_2(TEDGA)_2]^{2+}$ complex in Figure S13, the g tensor of the two KDs are collinear with z along the yle bond and $\|\mathbf{M}_{z,nn}\|^2 = \frac{1}{2}g_{n\|}^2$ and $\|\mathbf{M}_{\perp,nn}\|^2 = \frac{1}{2}g_{n\perp}^2$, $g_{n\|}$ and $g_{n\perp}$ being the axial and equatorial g factors of KDn. Then Eq.(S6) can be written as

$$\Delta\chi_{ax} = N_A\mu_0\mu_B^2\left[\frac{\left(e^{\Delta/2kT}\Delta g_1^2 + e^{-\Delta/2kT}\Delta g_2^2\right)}{4kT\left(e^{\Delta/2kT} + e^{-\Delta/2kT}\right)} + \frac{\left(e^{\Delta/2kT} - e^{-\Delta/2kT}\right)\Delta M_{12}^2}{\Delta\left(e^{\Delta/2kT} + e^{-\Delta/2kT}\right)}\right] \tag{S7}$$

where $\Delta g_n^2 = g_{n\|}^2 - g_{n\perp}^2$. Fitting the values of $\Delta\chi_{ax}$ deduced from AIS as a function of temperature with Eq.(S7) provides the values of Δg_1^2, Δg_2^2, ΔM_{12}^2 and Δ. Δg_1^2 and Δg_2^2 characterize the magnetic anisotropy of KD1 and KD2, ΔM_{12}^2 the anisotropic Van Vleck interaction between the two KDs and Δ their energy separation.

In the limit where $\Delta \gg kT$, KD2 is not thermally populated and Eq.(S7) reduces to

$$\Delta\chi_{ax} = N_A\mu_0\mu_B^2\left[\frac{\Delta g_1^2}{4kT} + \frac{\Delta M_{12}^2}{\Delta}\right] \tag{5}$$

The first term is a Curie term due to KD1 and KD2 brings only a TIP (Temperature Independent Paramagnetism) contribution. In this case, $\Delta\chi_{ax}T$ is a straight line. The slope gives the value of Δg_1^2 and the intercept $\dfrac{\Delta M_{12}^2}{\Delta}$. Since KD2 is not populated, one can not determine Δg_1^2 from the temperature dependence.

The equations for $\Delta\chi_{rh}$ are the same as Eqs. (S7) and (5) replacing Δg_1^2, Δg_2^2 and ΔM_{12}^2 by their rhombic counterparts: $\Delta g_{nrh}^2 = g_{nx}^2 - g_{ny}^2$ and $\Delta M_{rh12}^2 = \|\mathbf{M}_{x,12}\|^2 - \|\mathbf{M}_{y,12}\|^2$.

Non Kramers Doublet (NKD) model for $5f^2$ actinyl complexes

In the $[Pu^{VI}O_2]^{2+}$ complexes, the two lowest states are almost degenerate (with a gap Δ) and are well separated in energy from other as shown in Table S26. Eq.(S6) reduces to the second term, the so-called Van Vleck term within the two components of the NKD. Furthermore, a NKD has only one non zero g value, $g_\parallel$ along the z direction, $\|\mathbf{M}_{z,12}\|^2 = \frac{1}{2}g_\parallel^2$ and the axial magnetic susceptibility can be written as

$$\Delta\chi_{ax} = N_A\mu_0\mu_B^2 \frac{e^{\Delta/2k_BT} - e^{-\Delta/2k_BT}}{2\Delta\left(e^{\Delta/2k_BT} - e^{-\Delta/2k_BT}\right)} g_\parallel^2 \tag{S8}$$

Fitting of the values of $\Delta\chi_{ax}$ deduced from the variation of the AIS with temperature with Eq.(S8) provides the values for $g_\parallel$, the g factor of the NKD and Δ its energy splitting. From Table S27 it can be noticed that the interaction with the excited states introduces a small magnetization in the plane which is mostly from orbital contribution.

S4 Ab initio results

S4.1 $5f^1$ configuration

Table S20: Energy levels (in cm^{-1}) from the SF calculations for $5f^1$ complexes. The states are labelled according to the linear symmetry.

	CASSCF	CASPT2	RASSCF	RASPT2
$[Np^{VI}O_2]^{2+}$				
$^2\Phi$	0	0	0	0
$^2\Phi$	0	0	0	0
$^2\Delta$	1325	1175	1560	1388
$^2\Delta$	1325	1175	1560	1388
$^2\Pi$	23895	25025	25050	22075
$^2\Pi$	23895	25025	25050	22075
$[Np^{VI}O_2(TEDGA)_2]^{2+}$ XRD				
$^2\Delta$	0	0	0	0
$^2\Delta$	368	382	320	344
$^2\Phi$	1681	891	1264	589
$^2\Phi$	4006	4024	3575	3687
$^2\Pi$	18826	22267	19448	19828
$^2\Pi$	18900	23830	19602	20921
$[Np^{VI}O_2(TEDGA)_2]^{2+}$ 6c(CCC)				
$^2\Delta$	0	0	0	0
$^2\Delta$	418	390	352	300
$^2\Phi$	1851	1276	1416	860
$^2\Phi$	3597	3585	3157	3160
$^2\Pi$	18834	23340	19481	20442
$^2\Pi$	18957	23513	19632	20707
$[Np^{VI}O_2(TEDGA)_2]^{2+}$ 6c(TTT)				
$^2\Delta$	0	0	0	0
$^2\Delta$	511	609	452	522
$^2\Phi$	1858	1224	1434	775
$^2\Phi$	3665	3630	3238	3210
$^2\Pi$	19025	23758	19651	20749
$^2\Pi$	19081	23922	19786	21133
$[Np^{VI}O_2(TEDGA)_2]^{2+}$ 5c(TTT)				
$^2\Delta$	0	0	0	0
$^2\Delta$	527	727	462	628
$^2\Phi$	2486	2597	2033	2140
$^2\Phi$	3222	3499	2770	3041
$^2\Pi$	18885	23502	19533	20717
$^2\Pi$	18933	23713	19589	20843
$[Np^{VI}O_2(TEDGA)(H_2O)_2]^{2+}$ 5c(T)				
$^2\Delta$	0	0	0	0
$^2\Delta$	369	502	334	459
$^2\Phi$	1624	1205	1235	776
$^2\Phi$	3142	3365	2723	2899
$^2\Pi$	19478	23331	20180	21462
$^2\Pi$	19578	23450	20278	21588

Table S21: Energy levels (in cm^{-1}) from the SO calculations for $5f^1$ complexes. The states are labelled according to the linear symmetry.

	CASSCF	CASPT2	RASSCF	RASPT2
$[Np^{VI}O_2]^{2+}$				
$\Phi_{5/2}$	0	0	0	0
$\Delta_{3/2}$	3067	2963	3316	3122
$\Phi_{7/2}$	8151	8167	8060	8079
$\Delta_{5/2}$	9290	9175	9471	9337
$\Pi_{1/2}$	26949	28500	28275	25763
$\Pi_{3/2}$	30480	32121	31373	29020
$[Np^{VI}O_2(TEDGA)_2]^{2+}$ XRD				
$\Phi/\Delta_{5/2}$	349	0	0	0
$\Delta_{3/2}$	0	418	297	601
$\Delta/\Phi_{5/2}$	7021	7015	7038	7168
$\Phi_{7/2}$	9589	9579	9267	9465
$\Pi_{1/2}$	20468	24648	21371	22420
$\Pi_{3/2}$	23613	28074	24273	25484
$[Np^{VI}O_2(TEDGA)_2]^{2+}$ 6c(CCC)				
$\Phi/\Delta_{5/2}$	364	0	0	0
$\Delta_{3/2}$	0	424	357	637
$\Delta/\Phi_{5/2}$	7077	7070	7123	7253
$\Phi_{7/2}$	9356	9294	9054	9150
$\Pi_{1/2}$	20508	25164	21444	22741
$\Pi_{3/2}$	23655	28216	24346	25612
$[Np^{VI}O_2(TEDGA)_2]^{2+}$ 6c(TTT)				
$\Phi/\Delta_{5/2}$	403	0	0	0
$\Delta_{3/2}$	0	535	396	744
$\Delta/\Phi_{5/2}$	7093	7133	7138	7309
$\Phi_{7/2}$	9387	9320	9092	9183
$\Pi_{1/2}$	20642	25570	21578	23099
$\Pi_{3/2}$	23790	28623	24478	25980
$[Np^{VI}O_2(TEDGA)_2]^{2+}$ 5c(TTT)				
$\Phi/\Delta_{5/2}$	485	603	348	0
$\Delta_{3/2}$	0	0	0	484
$\Delta/\Phi_{5/2}$	7159	7157	7148	7183
$\Phi_{7/2}$	9291	9374	8902	9032
$\Pi_{1/2}$	20473	25048	21338	22496
$\Pi_{3/2}$	23603	28082	24225	25348
$[Np^{VI}O_2(TEDGA)(H_2O)_2]^{2+}$ 5c(T)				
$\Phi/\Delta_{5/2}$	0	0	0	0
$\Delta_{3/2}$	272	487	499	748
$\Delta/\Phi_{5/2}$	7047	7107	7213	7317
$\Phi_{7/2}$	9048	9160	8864	9005
$\Pi_{1/2}$	21180	25142	22259	23712
$\Pi_{3/2}$	24359	28242	25177	26603

Table S22: Composition (in %) of the SO states in terms of the SF ones, g-factors for the two lowest KDs and their energy gaps Δ (in cm^{-1}) in $5f^1$ complexes.

Method	KD	Φ	Δ	Π	g_x	g_y	g_z	Δ
$[Np^{VI}O_2(TEDGA)_2]^{2+}$ XRD								
SO-CASSCF	KD1	15	83	2	1.20	0.99	0.55	359
	KD2	60	39	0.7	1.08	0.95	2.92	
SO-CASPT2	KD1	64	35	0.2	0.80	1.10	3.18	418
	KD2	14	84	2	1.01	0.83	1.40	
SO-RASSCF	KD1	59	40	0.4	1.05	1.23	2.95	297
	KD2	18	80	2	1.45	1.21	0.60	
SO-RASPT2	KD1	70	30	0.1	0.66	0.97	3.57	601
	KD2	9	89	2	0.87	0.83	1.61	
$[Np^{VI}O_2(TEDGA)_2]^{2+}$ 6c(CCC)								
SO-CASSCF	KD1	76	22	2	1.17	1.13	0.13	364
	KD2	45	53	2	1.15	1.24	2.37	
SO-CASPT2	KD1	41	58	1	1.22	0.97	2.86	424
	KD2	79	20	1	1.14	1.32	0.63	
SO-RASSCF	KD1	37	62	1	1.20	1.07	3.12	357
	KD2	83	15	2	1.18	1.21	0.90	
SO-RASPT2	KD1	33	67	0	0.98	0.72	3.62	637
	KD2	85	13	2	0.87	0.84	1.58	
$[Np^{VI}O_2(TEDGA)_2]^{2+}$ 6c(TTT)								
SO-CASSCF	KD1	74	25	1	1.19	1.15	0.06	
	KD2	47	51	1	1.19	1.29	2.16	
SO-CASPT2	KD1	39	61	0	1.21	1.00	2.88	535
	KD2	80	18	2	1.19	1.25	0.76	
SO-RASSCF	KD1	39	61	0	1.26	1.13	2.93	396
	KD2	81	16	2	1.27	1.29	0.73	
SO-RASPT2	KD1	28	71	1	1.03	0.78	3.56	744
	KD2	89	9	2	0.97	0.99	1.48	
$[Np^{VI}O_2(TEDGA)_2]^{2+}$ 5c(TTT)								
SO-CASSCF	KD1	83	15	2	1.00	0.96	0.62	485
	KD2	39	59	2	1.00	1.06	2.97	
SO-CASPT2	KD1	78	20	1	1.13	1.00	0.10	603
	KD2	45	54	1	1.06	1.13	2.54	
SO-RASSCF	KD1	50	48	1	1.37	1.32	2.11	348
	KD2	70	28	2	1.42	1.48	0.19	
SO-RASPT2	KD1	59	40	1	1.35	1.09	1.81	484
	KD2	63	24	1	1.43	1.69	0.67	
$[Np^{VI}O_2(TEDGA)(H_2O)_2]^{2+}$ 5c(T)								
SO-CASSCF	KD1	51	48	1	1.21	1.32	2.16	272
	KD2	26	72	2	1.36	1.30	0.06	
SO-CASPT2	KD1	34	66		0.83	1.03	3.33	487
	KD2	12	86	2	0.84	1.05	1.40	
SO-RASSCF	KD1	26	74		0.62	0.75	3.90	499
	KD2	4	93	2	0.76	0.74	1.70	
SO-RASPT2	KD1	24	76		0.47	0.70	3.90	748
	KD2	4	94	2	0.70	0.67	1.82	

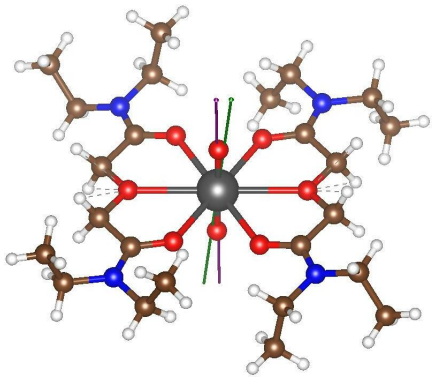

Figure S13: Main principal axis of the **g** tensors (g_z in Table S22) of KD1 (violet) and KD2 (green) in the $[Np^{VI}O_2(TEDGA)_2]^{2+}$ complex at SO-CASPT2 level of calculation. Color code: dark gray-Np, blue- N, red- O, saddle-brown- C, white- H.

Table S23: Energy differences (in kJ.mol^{-1}) between the conformers with different methods for $5f^1$ complexes.

	6c(CCC)	6c(TTT)	5c(TTT)
SF-CASSCF	26	0	22
SF-CASPT2	0	3	21
SF-RASSCF	26	0	23
SF-RASPT2	0	2	21
SO-CASSCF	25	0	22
SO-CASPT2	0	3	24
SO-RASSCF	26	0	24
SO-RASPT2	0	2	26
B3LYP	12	0	8

Table S24: *Ab initio* magnetic susceptibility tensor at 298 K in 10^{-8}m^3.mol^{-1} for the $5f^1$ complexes. S denotes the spin contribution.

	χ_x	χ_y	χ_z	$\Delta\chi_{ax}$	$\Delta\chi_{rh}$	χ_x^S	χ_y^S	χ_z^S	χ_m^S	$\Delta\chi_{ax}^S$
$[Np^{VI}O_2(TEDGA)_2]^{2+}$ 6c(TTT)										
SO-CASSCF	0.80	0.73	2.91	2.15	-0.07	-0.19	-0.23	-0.60	-0.34	-0.39
SO-CASPT2	0.76	0.61	4.70	4.01	-0.15	-0.15	-0.23	-0.66	-0.35	-0.46
SO-RASSCF	0.88	0.79	4.99	4.15	-0.09	-0.20	-0.26	-0.72	-0.39	-0.49
SO-RASPT2	0.74	0.58	5.56	4.89	-0.16	-0.11	-0.20	-0.77	-0.36	-0.61
$[Np^{VI}O_2(TEDGA)_2]^{2+}$ 6c(CCC)										
SO-CASSCF	0.80	0.73	2.97	2.20	-0.07	-0.19	-0.22	-0.63	-0.35	-0.42
SO-CASPT2	0.78	0.64	4.75	4.04	-0.14	-0.16	-0.22	-0.71	-0.36	-0.51
SO-RASSCF	0.88	0.80	5.16	4.32	-0.08	-0.20	-0.25	-0.75	-0.40	-0.52
SO-RASPT2	0.76	0.61	5.68	4.99	-0.15	-0.13	-0.20	-0.81	-0.38	-0.63
$[Np^{VI}O_2(TEDGA)_2]^{2+}$ 5c(TTT)										
SO-CASSCF	0.71	0.69	2.36	1.65	-0.02	-0.19	-0.18	-0.59	-0.32	-0.40
SO-CASPT2	0.65	0.61	2.23	1.59	-0.04	-0.17	-0.19	-0.51	-0.29	-0.33
SO-RASSCF	0.88	0.86	4.39	3.52	-0.02	-0.23	-0.25	-0.67	-0.38	-0.43
SO-RASPT2	0.86	0.80	3.65	2.82	-0.06	-0.21	-0.24	-0.58	-0.34	-0.36
$[Np^{VI}O_2(TEDGA)(H_2O)_2]^{2+}$ 5c(T)										
SO-CASSCF	0.82	0.75	4.49	3.70	-0.07	-0.20	-0.23	-0.74	-0.39	-0.51
SO-CASPT2	0.71	0.60	5.29	4.63	-0.11	-0.14	-0.21	-0.76	-0.37	-0.59
SO-RASSCF	0.73	0.67	6.17	5.46	-0.06	-0.16	-0.20	-0.85	-0.41	-0.67
SO-RASPT2	0.61	0.52	6.21	5.64	-0.09	-0.10	-0.16	-0.88	-0.38	-0.75

Table S25: Magnetic parameters for the 2 KDs model of Section S3.2 deduced from *ab initio* calculations for the $5f^1$ complexes. Δ in cm^{-1}, ΔM^2_{12} in μ^2_B.

method	Δg^2_1	Δg^2_2	ΔM^2_{12}	Δg^2_{rh1}	Δg^2_{rh2}	ΔM^2_{rh12}	Δ	$\Delta M^2_{12}/\Delta$	$\Delta M^2_{rh12}/\Delta$
$[Np^{VI}O_2(TEDGA)_2]^{2+}$ 6c(TTT)									
SO-CASSCF	-1.37	3.12	4.22	-0.09	0.24	-0.05	403	0.010	0.00003
SO-CASPT2	7.06	-0.92	2.77	0.13	0.13	0.08	536	0.005	0.00001
SO-RASSCF	7.18	-1.11	2.88	-0.30	0.05	0.05	397	0.007	0.00002
SO-RASPT2	11.83	1.24	0.75	-0.46	0.04	0.09	744	0.001	0.00000
$[Np^{VI}O_2(TEDGA)_2]^{2+}$ 6c(CCC)									
SO-CASSCF	-1.32	4.21	3.94	-0.11	0.21	-0.04	365	0.011	0.00003
SO-CASPT2	7.01	-1.14	2.82	-0.54	0.44	0.05	425	0.007	0.00002
SO-RASSCF	8.44	-0.63	2.44	-0.31	0.06	0.05	358	0.007	0.00002
SO-RASPT2	12.41	1.78	0.60	-0.45	-0.05	0.05	638	0.001	0.00000
$[Np^{VI}O_2(TEDGA)_2]^{2+}$ 5c(TTT)									
SO-CASSCF	-0.58	7.78	3.02	-0.08	0.13	-0.01	486	0.006	0.00001
SO-CASPT2	-1.14	5.25	3.81	0.15	0.15	-0.01	603	0.006	0.00001
SO-RASSCF	2.67	-2.09	4.43	-0.13	0.17	0.01	349	0.013	0.00004
SO-RASPT2	1.78	-2.01	4.66	-0.63	0.83	0.00	484	0.010	0.00002
$[Np^{VI}O_2(TEDGA)(H_2O)_2]^{2+}$ 5c(T)									
SO-CASSCF	3.06	-1.79	4.27	0.27	-0.17	-0.02	273	0.016	0.00006
SO-CASPT2	10.22	1.08	1.72	0.40	0.40	-0.05	488	0.004	0.00001
SO-RASSCF	14.76	2.32	0.08	0.19	-0.03	-0.03	500	0.000	0.00000
SO-RASPT2	14.91	2.86	-0.32	0.28	-0.05	-0.06	749	0.000	0.00000

S4.2 $5f^2$ configuration

Table S26: Energy levels (in cm^{-1}) from the SF and SO calculations for $5f^2$ free $[Pu^{VI}O_2]^{2+}$ cation and for the two TEDGA complexes .

$[Pu^{VI}O_2]^{2+}$				$[Pu^{VI}O_2(TEDGA)_2]^{2+}$				$[Pu^{VI}O_2(TEDGA)(H_2O)_2]^{2+}$			
CASSCF		CASPT2		CASSCF		CASPT2		CASSCF		CASPT2	
SF	SO	SF	SO	SF	SO	SF	SO	SF	SO	SF	SO
triplet		triplet		triplet		triplet		triplet		triplet	
0	0	0	0	0	0	0	0	0	0	0	0
0	0	1	0	18	1	342	7	12	2	90	43
3635	4489	3053	3138	1963	3551	2413	2935	1890	3540	1256	2705
6651	6977	4592	4857	6307	5681	5489	3775	6087	5827	4559	3816
6651	6978	4653	4899	6544	5811	5571	4173	6208	5859	4794	3832
20080	7542	15395	7585	18959	7998	16506	8130	18901	7846	16246	7949
23250	7542	26649	7585	19120	8031	24913	8153	19130	7874	23411	8021
singlet	13183	singlet	11173	singlet	12499	singlet	10432	singlet	12671	singlet	10157
10169	13271	6671	11709	9225	12749	6286	10441	9144	12706	6170	10691
12137	13271	7312	11716	9564	12818	7235	11439	9530	12793	6196	10966
12137	13780	7344	11773	9573	13431	7293	11524	9562	13743	6819	10998
12895	13781	9875	13315	11882	14862	7698	13383	11862	14523	7108	13143

Table S27: Ab initio magnetic susceptibility tensor at 298 K in 10^{-8}m^3.mol^{-1} for the $5f^2$ complexes. S denotes the spin contribution.

	χ_x	χ_y	χ_z	$\Delta\chi_{ax}$	χ_x^S	χ_y^S	χ_z^S	χ_m^S	$\Delta\chi_{ax}^S$
$[Pu^{VI}O_2(TEDGA)_2]^{2+}$ 6c(TTT)									
SO-CASSCF	0.17	0.17	14.01	13.84	0.07	0.07	-4.34	-1.40	-4.40
SO-CASPT2	0.18	0.18	13.52	13.35	0.07	0.07	-4.29	-1.38	-4.36
$[Pu^{VI}O_2(TEDGA)_2]^{2+}$ 6c(CCC)									
SO-CASSCF	0.17	0.17	14.00	13.83	0.07	0.07	-4.33	-1.40	-4.40
SO-CASPT2	0.17	0.17	13.52	13.35	0.07	0.07	-4.29	-1.38	-4.36
$[Pu^{VI}O_2(TEDGA)_2]^{2+}$ 5c(TTT)									
SO-CASSCF	0.17	0.17	14.01	13.85	0.07	0.07	-4.33	-1.40	-4.40
SO-CASPT2	0.17	0.17	13.83	13.66	0.07	0.07	-4.30	-1.39	-4.38
$[Pu^{VI}O_2(TEDGA)(H_2O)_2]^{2+}$ 5c(T)									
SO-CASSCF	0.17	0.17	14.00	13.808	-	-	-4.33	-	-4.33
SO-CASPT2	0.17	0.17	13.70	13.513	-	-	-4.24	-	-4.24
$[Np^{V}O_2(TEDGA)_2]^{+}$ 6c(TTT)									
SO-CASSCF	0.20	0.20	14.39	14.20	0.07	0.07	-4.37	-1.41	-4.44
SO-CASPT2	0.20	0.20	14.13	13.94	0.08	0.08	-4.35	-1.40	-4.42
$[Np^{V}O_2(TEDGA)_2]^{+}$ 5c(TTT)									
SO-CASSCF	0.20	0.20	14.44	14.24	0.07	0.07	-4.39	-1.41	-4.46
SO-CASPT2	0.20	0.20	14.38	14.18	0.078	0.08	-4.37	-1.401	-4.45

In this section, we attempt to analyze the RASSCF NKD wave functions of the free $[Pu^{VI}O_2]^{2+}$ cation and $[Pu^{VI}O_2(TEDGA)_2]^{2+}$ complex to determine the extent to which the wave functions and magnetic properties are affected by the two equatorial TEDGA ligands. The three active sets of orbitals comprise the metallic $5f_\delta$, $5f_\phi$ and the antibonding $5f_{\pi^*}$ orbitals along with the bonding and anti-bonding orbitals of the $[Pu^{VI}O_2]^{2+}$ moieties. The compositions of the ground SO NKD states $\{|1\rangle, |2\rangle\}$ of the $[Pu^{VI}O_2]^{2+}$ cation and $[Pu^{VI}O_2(TEDGA)_2]^{2+}$ complex are analyzed in Table S28. The SF wavefunctions are assigned to the irreps of the linear $[Pu^{VI}O_2]^{2+}$ moieties. Decomposition of the SO NKD states of the free $[Pu^{VI}O_2]^{2+}$ cation highlights significant admixing (almost 5%) of the energetically excited ^1G SF states with the dominant ^3H states due to high SOC of the plutonyl center. And as pointed out before, in the ligand field of two TEDGA the weights remain very little perturbed.[8]

The most dominant configurations of the multiconfigurational SF ^3H or ^1G states are listed in Table S28. The equatorial ligand field causes the energy degeneracy of the $5f_\phi$ and $5f_\delta$ orbitals to lift off, leading to the more stable $5f_\delta$ orbitals over the $5f_\phi$ orbitals those are undergoing antibonding interaction with the oxygen p orbitals as shown in Figure S14. Thus, the ground ^3H states of the $[Pu^{VI}O_2(TEDGA)_2]^{2+}$ complex exhibit more dramatic variations in the most dominant configurations and their weights than the free $[Pu^{VI}O_2]^{2+}$ cation. Notably, the ground wavefunctions are more strongly weighted on configurations where the unpaired electron occupies relatively more stable $5f_{\phi-}$ orbital avoiding the strong antibonding σ type interaction of the $5f_{\phi+}$ orbital with the ligands. Consequently the Mulliken spin population and the natural occupation analyses in the active 5f orbitals reflect the symmetry breaking of the two $5f_\phi$ orbitals where the ground triplet state of the ^3H can be denoted as $5f_{\delta+}^{(0.66)}5f_{\phi-}^{(0.66)}5f_{\delta-}^{(0.34)}5f_{\phi+}^{(0.34)}$ and the first excited triplet state as $5f_{\delta-}^{(0.66)}5f_{\phi-}^{(0.66)}5f_{\delta+}^{(0.34)}5f_{\phi+}^{(0.34)}$ where inside (), occupation numbers are given.

This detailed analysis of the NKD states in the plutonyl complexes shows the dramatic impacts of the ligand field on the nature of the ground SF states which might in turn affect the magnetic properties, but are nonetheless only mildly disrupted in comparison to their $5f^1$ counterpart. The $g_\parallel$ of the NKD of the free $[Pu^{VI}O_2]^{2+}$ cation from SO-RASSCF calculation is close to 6.09 whereas in the $[Pu^{VI}O_2(TEDGA)_2]^{2+}$ it is 5.92 (reduced by 2.8%) and previously we reported 5.89 (reduced by 3.3%) for $[Pu^{VI}O_2(DPA)_2]^{2-}$.[2] The $g_\parallel$ obtained from the fitting of the temperature dependent pNMR shifts for both the complexes is close to 4.8 to 5.0 (20% reduction), hence *ab initio* calculations overestimate. Unless this decrease, the magnetic moment of the central $[Pu^{VI}O_2]^{2+}$ cation is appreciably stable in a ligand field which satisfies the criteria for being a good probe in the structural analyses in solution.

Table S28: Percentage contributions of the SF states to the ground NKD $\{|1\rangle, |2\rangle\}$ in the free $[Pu^{VI}O_2]^{2+}$ cation and the $[Pu^{VI}O_2(TEDGA)_2]^{2+}$ complex from SO-RASSCF calculations. The dominant configurations in the multiconfigurational SF states are provided.

SF states	Configurations	$\|1\rangle$	$\|2\rangle$
	$[Pu^{VI}O_2]^{2+}$		
^3H	43% $5f^{\uparrow}_{\phi+}5f^{\uparrow}_{\delta+}$; 43% $5f^{\uparrow}_{\phi-}5f^{\uparrow}_{\delta-}$	47.6%	47.6%
^3H	43% $5f^{\uparrow}_{\phi-}5f^{\uparrow}_{\delta+}$; 43% $5f^{\uparrow}_{\phi+}5f^{\uparrow}_{\delta-}$	47.6%	47.6%
^1G	39%$f^{\uparrow\downarrow}_{\delta+}$; 38% $f^{\uparrow\downarrow}_{\delta-}$ 5% $f^{\uparrow}_{\phi-}f^{\downarrow}_{\pi-}$; 5% $f^{\uparrow}_{\phi+}f^{\downarrow}_{\pi+}$	0.0%	3.7%
^1G	76% $f^{\uparrow}_{\delta+}f^{\downarrow}_{\delta-}$; 5% $f^{\uparrow}_{\phi+}f^{\downarrow}_{\pi-}$ 5% $f^{\uparrow}_{\phi-}f^{\downarrow}_{\pi+}$	3.7%	0.0%
	$[Pu^{VI}O_2(TEDGA)_2]^{2+}$		
^3H	30% $5f^{\uparrow}_{\delta-}5f^{\uparrow}_{\phi+}$; 57% $5f^{\uparrow}_{\delta+}5f^{\uparrow}_{\phi-}$	46.3%	46.2%
^3H	56% $5f^{\uparrow}_{\delta-}5f^{\uparrow}_{\phi-}$; 31% $5f^{\uparrow}_{\delta+}5f^{\uparrow}_{\phi+}$	46.2%	46.3%
^1G	35%$f^{\uparrow\downarrow}_{\delta-}$; 40% $f^{\uparrow\downarrow}_{\delta+}$ 5% $f^{\uparrow}_{\phi-}f^{\downarrow}_{\pi-}$; 4% $f^{\uparrow}_{\phi+}f^{\downarrow}_{\pi+}$	4.9%	0.3%
^1G	75% $f^{\uparrow}_{\delta-}f^{\downarrow}_{\delta+}$; 6% $f^{\uparrow}_{\phi-}f^{\downarrow}_{\pi+}$ 4% $f^{\uparrow}_{\phi+}f^{\downarrow}_{\pi-}$	0.3%	5.0%

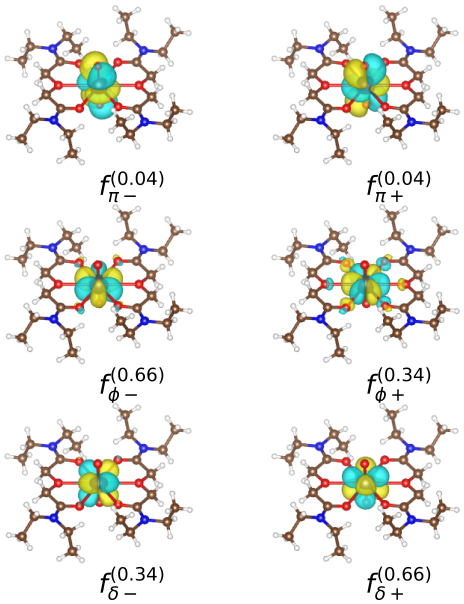

Figure S14: RASSCF active natural orbitals and their occupation numbers for the ground triplet state of the $[Pu^{VI}O_2(TEDGA_2]^{2+}$ complex. The isovalue is 0.14 e^-/bohr^3.

Table S29: The only non-zero g-factor $g_{\|}$ of the ground NKD in the $5f^2$ complexes.

	SO-CASSCF	SO-CASPT2
$[Pu^{VI}O_2]^{2+}$	6.10	6.11
$[Pu^{VI}O_2(DPA)_2]^{2-}$	5.89	5.73
$[Pu^{VI}O_2(TEDGA)_2]^{2+}$	5.93	5.79
$[Pu^{VI}O_2(TEDGA)(H_2O)_2]^{2+}$	5.95	5.89
$[Np^{V}O_2(TEDGA)_2]^{+}$	5.93	5.79

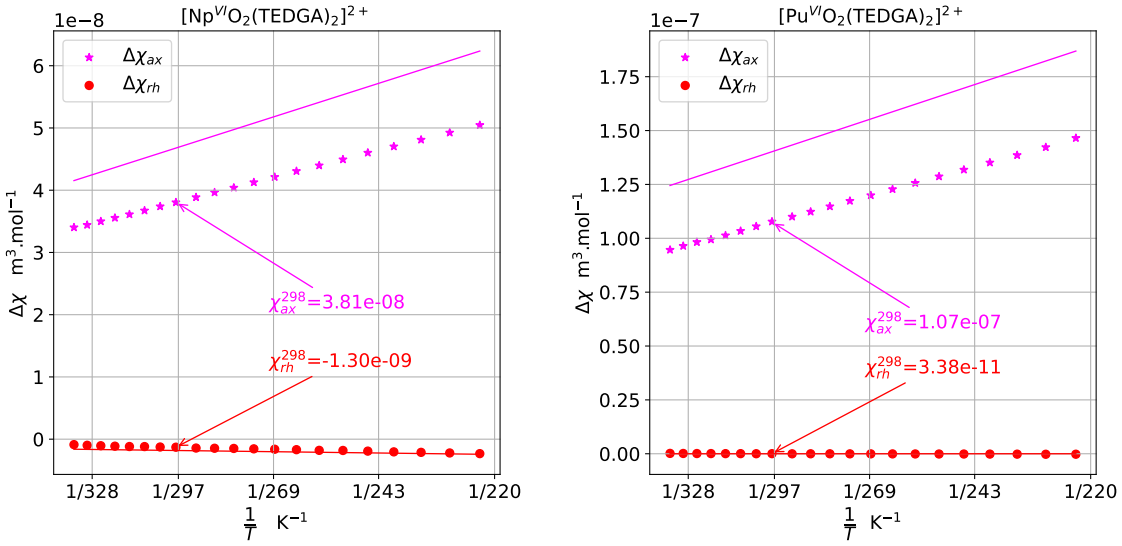

Figure S15: $\Delta\chi_{ax}$ (magenta) and $\Delta\chi_{rh}$ (red) *vs* 1/T (K^{-1}) from SO-CASPT2 (solid lines) and from the fit of experimental AIS (points) for the $[Np^{VI}O_2(TEDGA)_2]^{2+}$ (left) and $[Pu^{VI}O_2(TEDGA)_2]^{2+}$ (right) complexes in 6c(TTT) conformation.

References

(1) Poulin-Ponnelle, C.; Duvail, M.; Dumas, T.; Berthon, C. Contribution of Molecular Dynamics in pNMR for the structural determination of An^{V} and An^{VI} complexes in solution. *Inorg. Chem.* **2022**, *61*, 15895—15909.

(2) Autillo, M.; Islam, M. A.; Héron, J.; Guérin, L.; Acher, E.; Tamain, C.; Illy, M.-C.; Moisy, P.; Colineau, E.; Griveau, J.-C.; Berthon, C.; Bolvin, H. Temperature Dependence of ^{1}H Paramagnetic Chemical Shifts in Actinide Complexes, Beyond Bleaney's Theory:

The $An^{VI}O_2^{2+}$-Dipicolinic Acid Complexes (An=Np, Pu) as an Example. *Chemistry – A European Journal* **2021**, *24*, 7138–7153.

(3) Lefrançois, L.; Hebrant, M.; Tondre, C.; Delpuech, J.-J.; Berthon, C.; Madic, C. Z,E Isomerism and hindered rotations in malonamides: an NMR study of N,N'-dimethyl-N,N'-dibutyl-2-tetradecylpropane-1,3-diamide. *J. Chem. Soc., Perkin Trans. 2* **1999**, 1149–1158.

(4) Bertini, I.; Luchinat, C.; Parigi, G. Magnetic susceptibility in paramagnetic NMR. *Prog. Nucl. Magn. Reson. Spectrosc.* **2002**, *40*, 249–273.

(5) Bertini, I.; Luchinat, C.; Parigi, G.; Ravera, E. *NMR of Paramagnetic Molecules. Applications to Metallobiomolecules and Models*, 2nd ed.; Current Methods in Inorganic Chemistry; Elsevier Science, 2016; Vol. 2.

(6) Branch, M. A.; Coleman, T. F.; Li, Y. A Subspace, Interior, and Conjugate Gradient Method for Large-Scale Bound-Constrained Minimization Problems. *SIAM J. Sci. Comput.* **1999**, *21*, 1–23.

(7) Cornilescu, G.; Marquardt, J. L.; Ottiger, M.; Bax, A. Validation of Protein Structure from Anisotropic Carbonyl Chemical Shifts in a Dilute Liquid Crystalline Phase. *J. Am. Chem. Soc.* **1998**, *120*, 6836–6837.

(8) Gendron, F.; Pritchard, B.; Bolvin, H.; Autschbach, J. Magnetic Resonance Properties of Actinyl Carbonate Complexes and Plutonyl(VI)-tris-nitrate. *Inorg. Chem.* **2014**, *53*, 8577–8592.